Łódź University
Faculty of Physics and Chemistry
Department of Theoretical Physics

Simulation of the Muon Trigger for the Backing Calorimeter (ZEUS Experiment)

Michał Własenko
wlasenek@mail.desy.de

M.Sc. thesis
written under supervision of
Prof. Jacek Ciborowski

July 2004

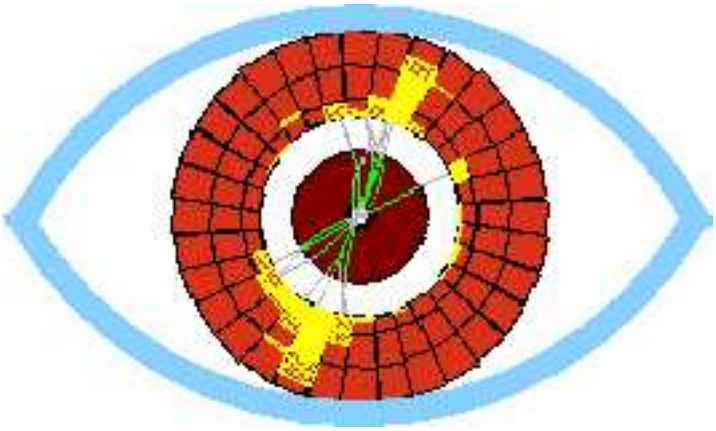

Figure 1: ZEUS is watching

Acknowledgments

I am extremely grateful to the many people without whose help this thesis could never have been written. Let every member of the Backing Calorimeter group accept my deep gratitude for their help and patience for my never-ending questions, also my appreciation of your dedication to your work is boundless.

In particular I would like to thank Grzegorz Grzelak for coordinating my efforts, offering numerous suggestions of improvements to the text and being the kind of a scientist that I aspire to become some day. Paweł Pluciński introduced me to the idea and complexities of the BAC and the trigger, always with humor and a glint in his eyes. Paweł Łużniak answered to my every question about physics and computer systems calmly and was a great bridge partner. Łukasz Ślusarczyk was a graceful guide to the world of Linux. Thank you all.

Most of all I would like to thank my supervisor - Prof. Jacek Ciborowski for his patronage, encouragement, editorial works and inviting me to join the ZEUS collaboration.

Last but not least I wish to thank Alicja Stelmach, my secondary school physics teacher, for encouraging me to study physics. Her class was a start of it all for me.

Contents

1 Introduction

1.1 General remarks

This thesis presents a Monte Carlo simulation of the muon trigger for the *Backing Calorimeter (BAC)*, which is a component of the *ZEUS* detector operating at the *Deutsches Elektronen Synchrotron (DESY)* in Hamburg, Germany. The ZEUS detector, located at an intersection of colliding electron (or positron) and proton beams of the HERA collider, is dedicated to investigate issues regarding the structure of the proton, photon and pomeron as well as to deliver data for testing numerous theoretical ideas motivated (mainly) by the Standard Model. Years 2000 ÷ 2002 brought a major upgrade of the accelerator with the aim to increase its luminosity by almost one order of magnitude. In the same time several detectors were also improved, in order to make better use of the scientific potential offered by the modernized collider. The Backing Calorimeter group decided to implement the BAC muon trigger system and include it in the ZEUS Global Trigger system.

The trigger is an important element of every high energy physics experiment. Its aim is to decide in the real time which events are accepted for the further off-line analysis. The BAC trigger system works using digital information from proportional wire chambers, applies a muon recognition algorithm to exclude background events and sends a positive decision to the ZEUS Global Trigger only if a muon-like signal was identified in the BAC.

The Monte Carlo chain for ZEUS is a software package for the complete simulation of the *ep* interactions in the detector. At first, a file with chosen *ep* processes is delivered by the Monte Carlo generator. Next, the response of each of the detector components to the products of the *ep* interaction is generated by the *MOZART* program, the trigger decision and the off-line reconstruction results are simulated. The trigger is simulated by the *CZAR/ZGANA* package. The *BACFLT* set of routines is the muon trigger simulation for the Backing Calorimeter, implemented by the author of this thesis.

Implementation and efficiency studies of the BAC muon trigger were performed using samples of events with heavy vector mesons ($\Upsilon, J/\Psi, \Psi'$),

beauty quarks, and the Bethe-Heitler process, all with muons in the final states.

1.2 $e^{\pm}p$ physics at HERA

After more than 3 decades of investigations a lot of experimental results have been obtained allowing to create a reasonable model of the proton at the partonic level. In simple words, it is build of three valence quarks (u, u, d) and a sea of quarks and antiquarks $(u\overline{u}, d\overline{d}, s\overline{s}, ...)$ which all are bound with gluons. The proton is a dynamical system of partons confined by the color forces described by the Quantum Chromodynamics (QCD). The most suitable process to study the proton is deep inelastic scattering (see below) which in the past has been done using neutrino and e, μ beams on stationary targets. HERA is the first $e^{\pm}p$ collider, allowing to reach center-of-mass energies exceeding 300 GeV.

Electron[1] -proton interactions (Fig. 2) proceed via exchange of virtual vector bosons $(\gamma, Z^0, W^{\pm})$ which are the carriers of the electro-weak force. Processes mediated by the γ and Z^0 gauge bosons are called *Neutral Currents (NC)*, and by $W^{\pm}$ - *Charged Currents (CC)*. Due to the conservation of the lepton number, the final products are: scattered lepton l, and the hadronic final state X:

$$ep \rightarrow lX. \tag{1}$$

The usual variables used to describe the lepton proton scattering kinematics are:

$$Q^2 = -q^2 = -(k - k')^2, \tag{2}$$

$$s = (k + P)^2, \tag{3}$$

$$W^2 = (q + P)^2 = p^2, \tag{4}$$

$$x = \frac{Q^2}{2P \cdot q}, \tag{5}$$

$$y = \frac{q \cdot P}{k \cdot P}, \tag{6}$$

where k, k', P represent four vectors of the initial and the final lepton and of

[1]From now on positrons and electrons will be both referred to as 'electrons'.

the incoming proton, respectively. q is the four-momentum of the intermediate boson, x is a fraction of the proton four momentum carried by the parton interacting with the electron, y is a fraction of the electron four momentum carried by the boson. Variables s and W^2 are the center-of-mass energy squared of the electron-proton and intermediate boson-proton systems, respectively. The positive value of of the four momentum transfer squared, $Q^2 = -q^2 > 0$, determines the hardness of the interaction. The Lorentz invariant variables: Q^2, x and y are related by $Q^2 = xys$. The resolution of the virtual boson (its wavelength) is given by:

$$\Delta z \sim \frac{\hbar c}{\sqrt{Q^2}} \approx \frac{0.2}{\sqrt{Q^2\ [GeV^2]}} fm, \tag{7}$$

which with HERA center-of-mass 318 GeV energy reaches $\sim 10^{-3}\ fm$.

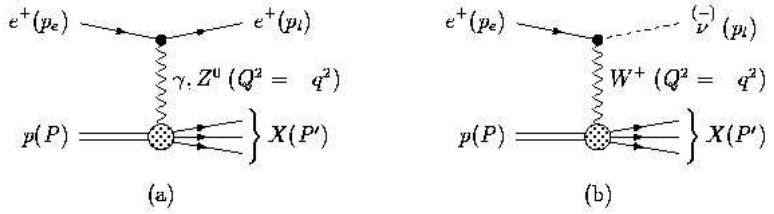

Figure 2: Electron-proton interactions: Neutral Current (NC) *(a)* and Charged Current (CC) *(b)* processes

The basic distinction of the kinematic regimes in the *ep* scattering is done using the Q^2 variable. Processes with $Q^2 \approx 0$ are called *photoproduction (PHP)*. If Q^2 is much larger then the proton mass squared, we talk about *deep inelastic scattering (DIS)*.

The differential cross section for the one boson exchange (neutral current) deep inelastic scattering $e^{\pm}p \to e^{\pm}X$ is given by [13]:

$$\frac{d^2\sigma^{NC}(e^{\pm}p)}{dxdQ^2} = \frac{2\pi\alpha^2}{xQ^4}\{Y_+F_2^{NC}(x,Q^2) - y^2F_L^{NC}(x,Q^2) \mp Y_-xF_3^{NC}(x,Q^2)\}, \tag{8}$$

where $Y_{\pm} = 1 \pm (1-y)^2$, and α is the QED coupling constant. The neutral

current structure functions are:

$$F_2^{NC}(x,Q^2) = \sum_f xA_f(Q^2)[q_f(x,Q^2) + \overline{q}_f(x,Q^2)], \tag{9}$$

$$xF_3^{NC}(x,Q^2) = \sum_f xB_f(Q^2)[q_f(x,Q^2) - \overline{q}_f(x,Q^2)], \tag{10}$$

and

$$F_L^{NC} \;=\; F_2^{NC} \;-\; 2xF_1^{NC}, \tag{11}$$

where $q_f(x,Q^2)$ are parton density functions (PDFs), i.e. probabilities of finding a quark of flavor f, with momentum fraction x at given Q^2 and the prefactors $A_f(Q^2)$ and $B_f(Q^2)$ are defined as:

$$A_f(Q^2) = e_f^2 - 2v_e v_f e_f P_z + (v_e^2 + \alpha_e^2)(v_f^2 + \alpha_f^2)P_z^2, \tag{12}$$

$$B_f(Q^2) = -2\alpha_e \alpha_f e_f P_z + 4v_e \alpha_e v_f \alpha_f P_z^2, \tag{13}$$

with

$$P_z = \frac{1}{4sin^2\Theta_W cos^2\Theta_W} \cdot \frac{Q^2}{Q^2 + M_Z^2}. \tag{14}$$

Here e_f is the electric charge of the struck quark, $v_{e/f}$ and $\alpha_{e/f}$ are the vector and axial-vector coupling constants for the lepton e and the quark f, respectively, Θ_W is the weak mixing angle and M_Z is the Z-boson mass.

The differential cross section with one boson exchange for unpolarized charged current deep inelastic scattering process $e^-p \to \nu X$ and $e^+p \to \overline{\nu}X$ are given by [14]:

$$\frac{d^2\sigma^{CC}(e^{\pm}p)}{dxQ^2} = \frac{G_F^2}{4\pi x}\frac{M_W^4}{(Q^2+M_W^2)^2}\{Y_+F_2^{CC}(x,Q^2) - y^2F_L^{CC}(x,Q^2) \mp Y_- xF_3^C C(x,Q^2)\}, \tag{15}$$

where $Y_\pm = 1 \pm (1-y)^2, G_F$ is the Fermi coupling constant and M_W is the mass of the W boson. [2] The charged current structure functions for $e^{\pm}p$ DIS are given by:

$$F_2^{CC}(x,Q^2) = \sum_f xq_f(x,Q^2) + \sum_f x\overline{q}_f(x,Q^2), \tag{16}$$

$$xF_3^{CC}(x,Q^2) = \sum_f xq_f(x,Q^2) - \sum_f x\overline{q}_f(x,Q^2), \tag{17}$$

[2] In the thesis, units in which $\hbar = c = 1$ are used.

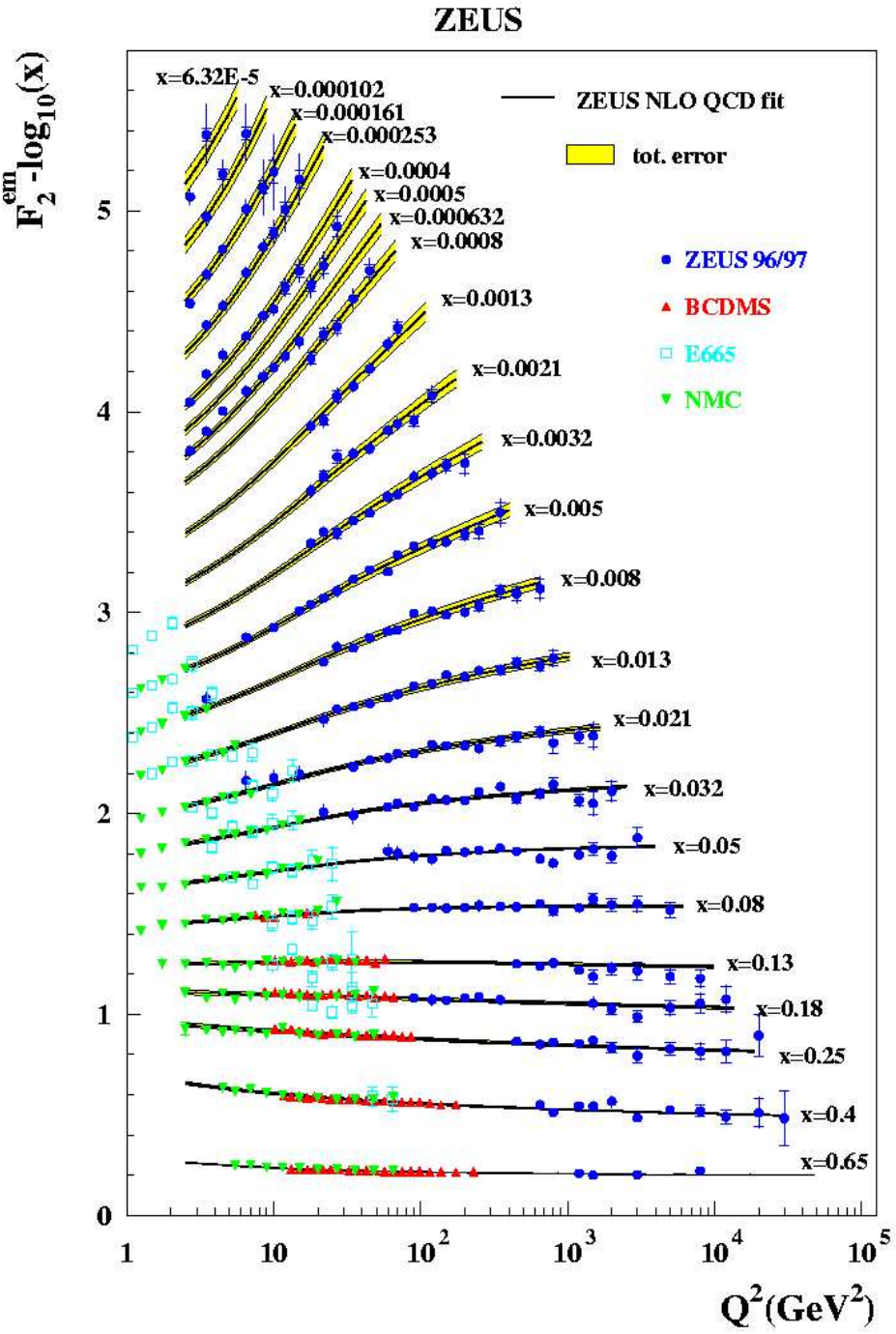

Figure 3: Compilation of the proton structure function F_2 measurements in a wide range of x, measured by ZEUS and other experiments [25].

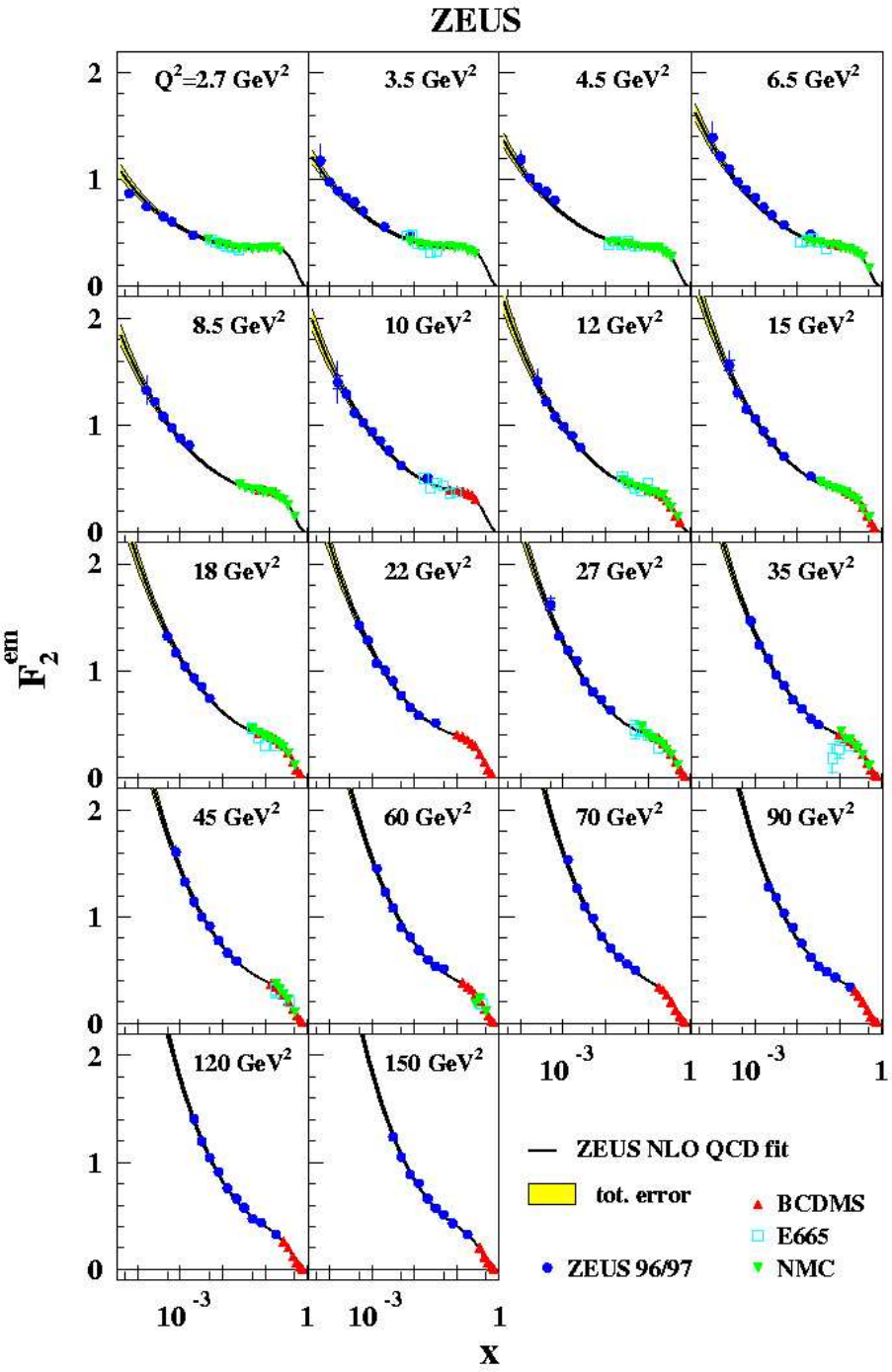

Figure 4: The compilation of the $F_2(x, q^2)$ proton structure functions, at fixed Q^2 measured by ZEUS and other experiments [25].

The parton density functions $q_f(x, Q^2)$ cannot be derived form first principles and have to be determined from experiments by measureing structure functions $F(x, Q^2)$. A compilation of the proton structure function $F_2(x, Q^2)$ measurements from ZEUS and other experiments is shown in Fig.3 [25]. In particular new measurments from HERA in the low-x region demonstrated a strong rise of $F_2(x, Q^2)$ towards low values of x, at fixed Q^2 (see Fig. 4) [25]. This observation indicates that the sea quark density at low x is high while the strong coupling constant, $\alpha_s(Q^2)$ is rather small. Another interesting discovery was the strong rise of $F_2(x, Q^2)$ with Q^2, at fixed x (see Fig. 3), in agreement with the perturbative QCD (pQCD).

Electron-proton scattering at $Q^2 \approx 0$ can be viewed as scattering of an almost real photon and is called *photoproduction (PHP)* [3]. Photoprocuction γp is characterized by much larger cross section than DIS and is a source of high statistics data regarding numerous physical issues. The basic measurement is the total γp cross section [29] which is confronted with theoretical predictions based on the QCD and on the Regge inspired models. It has been known since a long time that the γp interaction resembles hadron-p interactions. This is explained assuming that the photon has a pure electromagnetic as well as a hadronic component, the latter manifesting during interactions with hadrons (both inclusive and exclusive processes). The hadronic state of the photon is described in a class of models based on the Vector Meson Dominance concept (and various extensions) or in terms of its partonic structure, i.e. in the language of the QCD. This composite photon is called *resolved*, contrary to the point-like photon, called *direct*. Virtual photons ($Q^2 \gg 0$) can also be viewed in this picture but the proportion of resolved and direct components decreases strongly with growing virtuality.

In ep interactions also diffractive processes are observed. *Diffraction* in high energy physics is a process in which no quantum numbers are exchanged between colliding particles (only spin can be exchanged). The hadron-hadron diffraction is well described within the Regge phenomenology [19, 20], which is also applicable for the $\gamma p(\gamma^\star p)$ scattering. Diffraction can be split into 3 basic classes:

[3] The scattered electron is detected in a calorimeter located $\sim$ 100 m down the beam line.

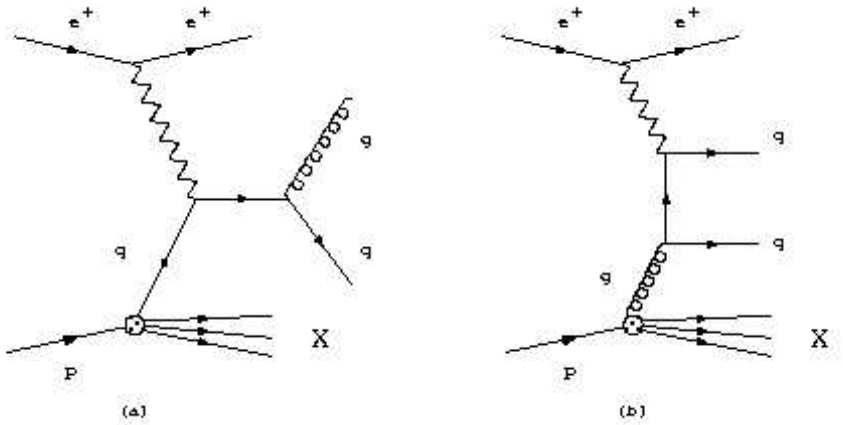

Figure 5: Leading order direct photon processes: QCD Compton *(a)* and Boson-Gluon Fusion *(b)*

- *elastic* scattering, when the same particles emerge from the collision,
- *single dissociation*, in which one of the initial state particles disintegrates into a multi-particle final state,
- *double dissociation*, when both particles dissociate.

The signature of a diffractive event (Fig. 7) is a *large (pseudo)rapidity gap* between the final state hadron jets X and Y, where the pseudorapidity of a single particle is defined as:

$$\eta = -ln\ tan\frac{\theta}{2}, \tag{18}$$

θ being the polar angle relative to the initial direction of the incoming particles. In non-diffractive ep interactions hadrons populate uniformly the entire rapidity space.

Diffractive processes proceed through an exchange of a pomeron $\mathbb{P}$ - an object with vacuum quantum numbers. In the simplest picture the pomeron can be seen as a virtual, color neutral gluon pair. In the diffractive $\gamma^{\star}p$ processes a virtual photon emitted by the electron interacts with the pomeron emitted from the proton. Diffraction is interesting from the point of view of

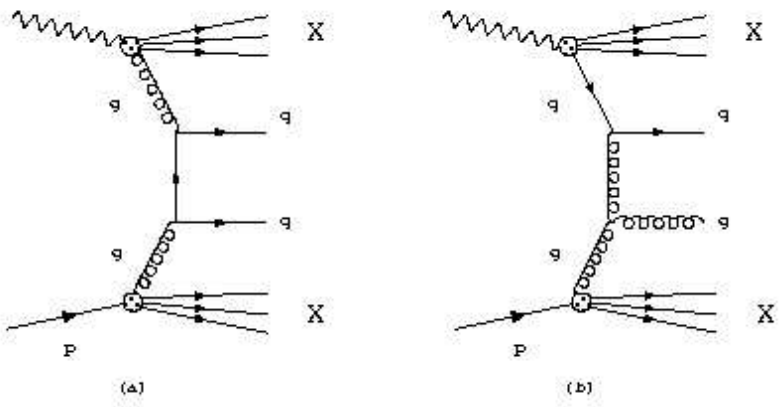

Figure 6: Examples of leading order resolved photon processes

both Regge phenomenology as well as QCD. At sufficiently large Q^2, the diffractive $\gamma^\star p$ scattering is a tool to study the partonic structure of the pomeron (deep inelastic $\gamma^\star \mathbb{P}$ scattering).

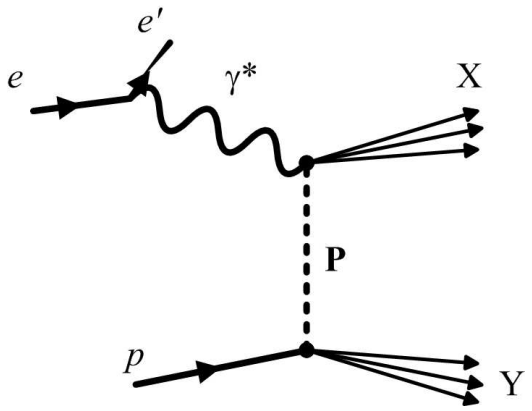

Figure 7: Example of double dissociation diffractive *ep* scattering.

Testing the muon trigger of the Backing Calorimeter requires anaylyzing events with muons in the final state. Muons emerge from numerous processes in *ep* collisons. They may be produced directly, e.g. in the Bethe-Heitler process, or appear as products of heavy quark decays. At HERA heavy quarks (c, b) are produced in numerous processes which provide an excellent

field to test the predictions of the perturbative QCD. Production of c and b is studied in both PHP and DIS.

At the leading order, the *photon-gluon fusion* process plays the main role in charm and beauty production [4]. In this process the virtual photon interacts with a gluon from the proton giving a $q\overline{q}$ pair in the final state (Fig. 6):

$$\gamma + g \rightarrow q + \overline{q}. \tag{19}$$

which subsequently may form a vector meson. This channel contributes to about 80% of the total cross-section to charm and beauty production [17].

Heavy quarks may also be produced in diffractive processes like exclusive production of heavy vector mesons ($J/\Psi, \Upsilon$).

Initial state	Decay channel	Fraction
$J/\Psi_{\overline{c}c}(1S)$	$\mu^+\mu^-$	$(5.88 \pm 0.10)\%$
$\Psi_{\overline{c}c}(2S)$	$J/\Psi(1S)\pi^+\pi^-$	$(34.8 \pm 2.8)\%$
$\Upsilon_{\overline{b}b}(1S)$	$\mu^+\mu^-$	$(2.48 \pm 0.06)\%$
$\Upsilon_{\overline{b}b}(2S)$	$\mu^+\mu^-$	$(1.31 \pm 0.21)\%$

Table 1: Examples of heavy quarks bound states decays into muons.

For the purpose of this work samples of heavy vector meson ($\Upsilon_{\overline{b}b}, J/\Psi_{\overline{c}c}, \Psi'_{\overline{c}c}$), beauty quark production and additionally Bethe-Heitler process (with muons in the final states) were used to test the efficiency of the BAC muon trigger. Branching ratios for decays of selected heavy mesons with muons in the final state are shown in Table 1. These decay channels are used (among others) in physics analysis (e.g. cross section measurements).

[4] The contribution from the resolved (hadronic) component of the cross-section becomes important for large center-of-mass energy and small masses of the final state particles. In heavy quark production, this affects c production much more than b production.

2 HERA accelerator and ZEUS detector

2.1 HERA accelerator

HERA *(Hadron Elektron Ring Anlage)*, which is running since 1992 at DESY *(Deutsches Elektronen Synchrotron)* in Hamburg, is the only in the world electron-proton collider (Fig. 8, 9), accelerating beams of protons and electrons (or positrons), situated $10 \div 25$ meters underground, on the circumference of 6.3 *km*. The beams are pre-accelerated and collimated in a system of 6 smaller machines to the energies of 40 GeV (protons) and 14 GeV (electrons) and then injected into HERA, where final energies 920 GeV and 27.5 GeV are reached, respectively. The center-of-mass energy of the ep collisions is $\sqrt{s} \approx 318$ GeV, the typical instantaneous luminosity available at HERA is in the range of $1.0 \div 2.5 \cdot 10^{31}\ cm^{-2}\ s^{-1}$.

Figure 8: Shape of the HERA collider ring on the photography of Hamburg

The HERA tunnel contains two independent accelerating rings. The electron ring, constructed using the warm technology (operating in ambient temperatures), consists of 416 magnets, bending and collimating the beam and 82

accelerating cavities. The superconducting proton ring, operating in liquid helium at the temperature of 4.2 K, consists of 104 magnets with 2 accelerating cavities. In 2 opposite points on the circumference, where detectors the ZEUS and H1 are located, beam pipes merge into one and beams are brought to head-on collisions (at 180° angle). The electron beam is polarized up to 70% in the transverse direction.

Both beams have the structure of bunches. The position of the bunch in the beam is called bucket. Electron-proton interactions can take place when a filled electron and proton bucket meet. There are 220 possible buckets in each beam, but only about 180 are filled. The unpaired buckets are left for the background studies. The time interval between 2 bunch crossings is 96 ns, which defines the 10.4 MHz clock for the DAQ (Data AcQuisition) electronics systems of the experiments.

Four main experiments are using the HERA accelerator. ZEUS and H1 detectors make use of the ep collisions. They are designed to study proton structure functions in deep inelastic scattering, QCD studies, photon and pomeron structure as well as searches beyond the Standard Model. The HERMES detector makes use of polarized electron beam by colliding it with a polarized proton gas target to study the proton spin structure. The HERA-B detector uses wire targets inserted into the proton beam to study CP violation.

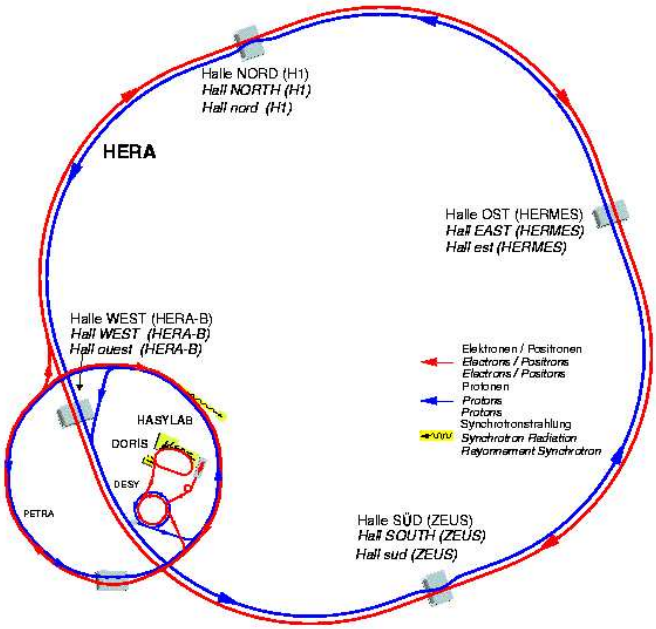

Figure 9: Scheme of the HERA collider ring

2.2 ZEUS detector

ZEUS (Fig. 10) is a complex, multipurpose detector designed to study several aspects of *ep* interactions. It is composed of over a dozen specialized components, each playing a significant role in reconstruction of the *ep* events. A brief description of the main components of the detector is given below.

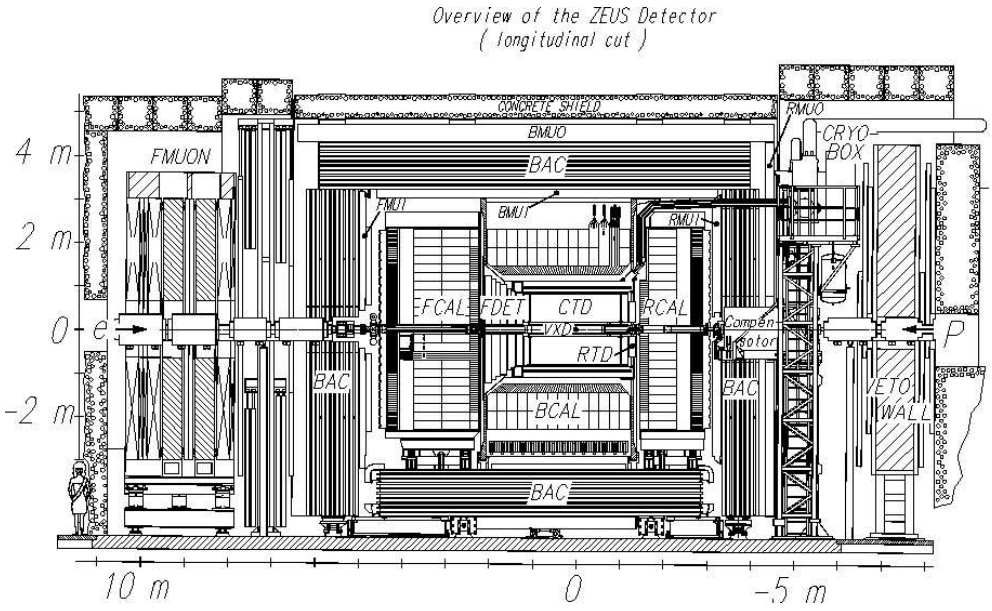

Figure 10: ZEUS detector scheme

The ZEUS coordinate system is a right-handed Cartesian system, with the Z axis pointing in the proton beam direction, referred to as the "forward direction", and the X axis pointing left towards the center of HERA. The coordinate origin is at the nominal interaction point.

Starting from the interaction point, ZEUS detector consists of following components:

- Micro Vertex Detector (MVD) is a silicon micro-strip tracking system. It is built of 3 layers of crossed Si sensors in a barrel, parallel to the beam direction and 4 layers in the forward endcap. Its high tracking precision (up to 10 microns) allows to reconstruct secondary vertices and improve identification of heavy quarks.

- The Central Tracking Detector (CTD) is a cylindrical drift chamber, covering the polar angle [5] from 15° to 164° and the full azimuthal angle. It consists of 9 so called 'super layers', each with 8 planes of sense wires. CTD was designed to reconstruct tracks of charged particles, measure their momenta, and identify them (by measuring the energy loss - dE/dx). CTD plays also the main role in vertex finding algorithms.

- The Forward Tracking Detector (FTD), Rear Tracking Detector (RTD) and Straw Tube Tracker (STT) were designed to supplement track measurement in directions almost parallel to the beam. Both FTD and RTD drift chambers, cover polar angels in the ranges of $7.5° \div 28°$ and $159° \div 170°$, respectively. STT, which is based on the technology of drift tubes, covers polar angels between 5° and 25°.

- All tracking detectors are surrounded by thin super-conducting solenoid, providing magnetic field of 1.8 T, which allows to measure momenta of charged particles using the track curvature.

- The uranium scintillator CALorimeter (CAL) covers about 99.8 % of the solid angle. CAL is a sampling calorimeter built of layers of depleted uranium and plastic scintillator. It is divided into electromagnetic and hadronic sections, both providing high energy resolution of:

$$\frac{\sigma_E}{E} \approx \frac{18\%}{\sqrt{E(GeV)}} \quad for\ electrons \tag{20}$$

and

$$\frac{\sigma_E}{E} \approx \frac{35\%}{\sqrt{E(GeV)}} \quad for\ hadrons. \tag{21}$$

- The Backing Calorimeter (BAC), covering almost full solid angle measures energy of hadrons not absorbed in CAL. The iron yoke bearing the

[5] The polar angle is measured in the zx plane, starting from the direction of the proton beam.

BAC closes the magnetic field of the solenoid. A detailed description of the BAC is given in Chapter 3.

- The Muon Chambers - B/R MUON (Barrel, Rear MUON) and FMUON (Forward Muon) detectors are dedicated to identify and measure momenta of muons. They consist of layers of streamer tubes and drift chambers, located on the inside and outside of the BAC iron yoke.
- The VETO wall - large iron wall (approx. 8 m high, $8m$ wide and 90 cm thick), covered with scintillators on both sides is placed in the rear area of the detector. The task of the VETO wall is to reject events induced by the proton beam halo.
- Finally, Luminosity Monitor (LUMI), installed in the HERA tunnel (107 m from the nominal interaction point), in the vicinity of the electron beam pipe measures instantaneous luminosity provided by the HERA accelerator. It measures the rate of bremsstrahlung event: $e^- p \rightarrow \gamma e^- p$, detecting the scattered electrons and the photons.

The readout and the trigger electronics of the ZEUS experiment is located the so called Rucksack - a three-storey building, placed next to the detector. It contains electronics that does not have to be placed on or within the detector, which prevents electronic circuits from radiation damage and makes servicing easier.

2.3 ZEUS Data selection system

The aim of the trigger of a high energy physics experiment is to select interesting physics events, and to on-line on-line reject background of unwanted events. The most interesting process measured in ZEUS - the Deep Inelastic Scattering has small cross-section, when the background rates are significant. ZEUS storage capacity is of $\mathcal{O}(10^8)$ events per year. Thus the goal of the ZEUS trigger system is to reduce the event rate to about 10 events per second (approx. 500 kB/s).
Each event has to fulfill predefined criteria of three trigger levels, before it is recorded on the Data Summary Tapes (DST). In the following, sources of background at HERA and all levels of the trigger system are described.

2.3.1 Sources of backgrounds at HERA

There are 3 important sources of background that the trigger has to reject:

- Background associated with the proton beam. Firstly, *off-momentum protons*, when causing showers of secondary particles when hitting parts of the beam pipe close to the beam, produce so called *beam-halo*. Secondly, particles produced by proton collisions with the *rest-gas* (H_2, O_2, CO, CO_2, etc.) in the beam pipe induce so called beam-gas events. These two classes constitute the main source of background at HERA, with a typical rate of these events, observed by the ZEUS detector, of $\mathcal{O}(50)kHz$. The rate of electron beam-gas events is much lower.

- *Cosmic rays*, are not such troublesome. The rate of cosmic rays events is of $\mathcal{O}(1)kHz$, but mainly they deposit low energy in the detector, so they are rejected by triggering with thresholds requirements and additional vertex positioning.

- Finally, certain class of *ep* interaction events - *photoproduction* - must be suppressed due to its high cross-section. It is associated with exchange of almost real photon (physics events with low Q^2), that for example implies production of light vector mesons. This kind of events result in a background of $\mathcal{O}(180)Hz$ and due to limited data storage ability cannot be all written on tapes.

2.3.2 The First Level Trigger (FLT)

The data from about 0.5 million channels of the detector components flows through the front-end electronics of the ZEUS components with the HERA bunch-crossing frequency, 10.4 *MHz*. This data-flow goes through analog (like in CAL) or digital pipelines (like in the BAC and tracking detectors) and and in parallel a subset of it is used to compute the local FLT decisions. Then each component sends its decision to the Global First Level Trigger (GFLT). The GFLT computes a word containing 64 bits and if at least one of them is positive, the overall positive GFLT decision is taken. Total time for all these operations is 5 μs per event, hence local components triggers

use very simple accept-reject algorithms. The output rate of FLT is designed to be of less then 1 *kHz*. The First Level Trigger is implemented on the hardware level using dedicated circuits.

2.3.3 The Second Level Trigger (SLT)

After receiving the 'accept' signal from the FLT, components compute their second level trigger local decisions and send them to the Global Second Level Trigger (GSLT) system. At this level, implemented using parallel microprocessors - IMMOS T800 Transputers, as the data volume is smaller then in FLT, there is more time (10 *ms*) for more complex accept-reject algorithms, both on the component and the GSLT side. Typical analyzed quantities are: angular distribution of energy deposits, number of tracks, muon hit patterns or vertex position and timings. The output rate of GSLT is less then 100 *Hz*.

2.3.4 The Event Builder (EVB) and the Third Level Trigger (TLT)

The Event Builder system broadcasts the 'accept' signal from GSLT to all components, receives full sets of data from them, packs it into the ADAMO data base tables (the standard ZEUS data base system), and sends it to the Third Level Trigger. TLT works on the farm of Silicon Graphics and PC Linux machines. It uses more sophisticated algorithms then FLT and SLT, to give a final decision whether the event should be recorded on Data Summary Tapes (DST). TLT system uses simplified physics filters - as they are used in data analysis, so the final rate is reduced to typically 5 *Hz*, which is equivalent to $0.5 \div 1.0$ *Mbyte/s* data transfer.

2.3.5 Reconstruction and Data Summary Tapes

All events accepted by the Third Level Trigger are written on the mass storage tapes. They form the so called 'raw data' sample, which is used for further off-line analysis. The reconstruction program ZEPHYR, reproduce physical observables out of raw data, using algorithms specific for each readout component to compute global quantities and writes the files onto Reconstructed Data Storage Tapes (RDST). The user has an access to both:

raw and reconstructed data (also on fast accessible hard disks in reduced format as mini-DST).

As the subject of this thesis is related to the upgrade of the BAC trigger system, in further only this component local trigger system will be described in details.

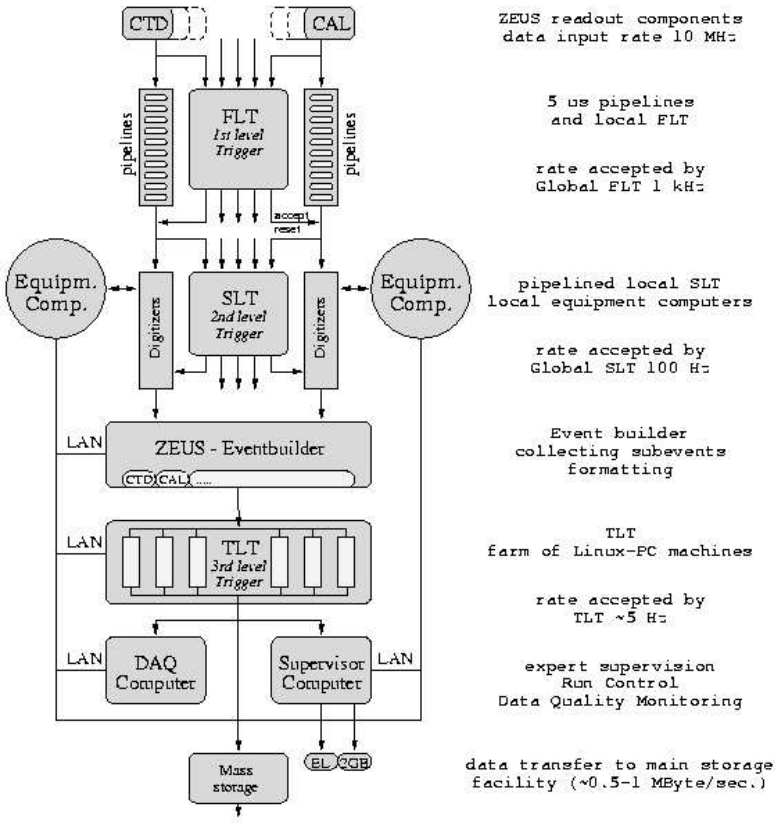

Figure 11: Scheme of the part of the ZEUS Trigger structure.

3 The Backing Calorimeter (BAC)

The motivation for constructing the Backing Calorimeter (BAC) in the ZEUS detector was twofold. Since the uranium calorimeter is not deep enough to contain all hadron cascades, the first aim of the BAC is to measure the energy of so called 'leakages' from CAL, making the total energy measurement more complete. And secondly, due to design of its active components (wire chambers) the BAC works as a muon tracking detector, supplementing the muon chambers in ZEUS. Electronics of the Backing Calorimeter is also designed to participate in the trigger system of the experiment. In the following, the main features of the logics of the readout and trigger systems are described.

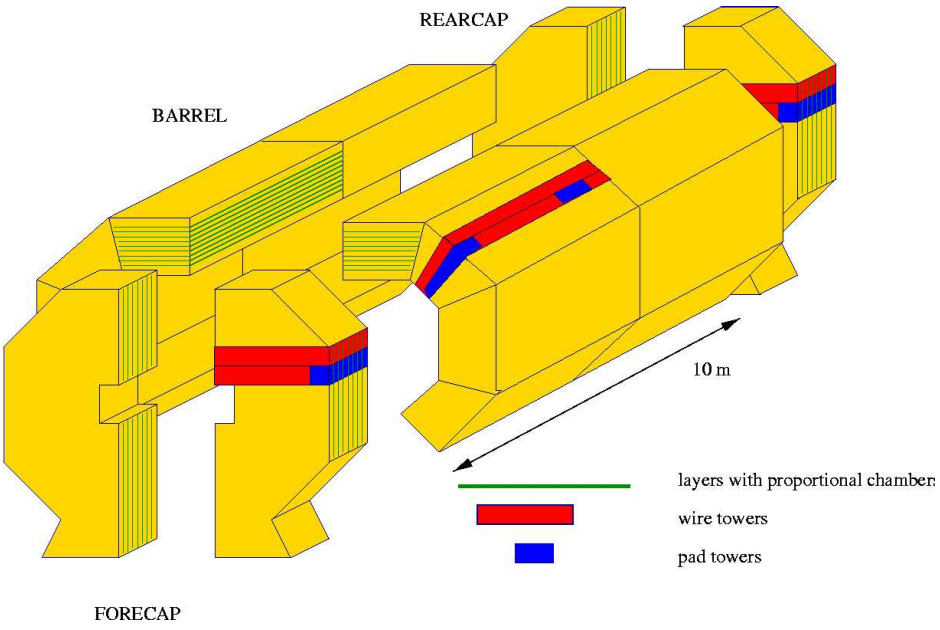

Figure 12: Main units of the BAcking Calorimeter detector

3.1 The design of BAC

Geometrically, the Backing Calorimeter (Fig.12) consists of 3 main units: the Forecap, the Rearcap and the Barrel. The BAC is a sampling calorimeter composed of 7 to 10 layers of proportional gas drift chambers with iron

plates as the absorber, which also serve as the yoke of the detector. A single chamber (Fig. 13) is an aluminum box, of 13.5 $\times$ 1.1 cm transverse dimensions, 2 to 7 m long. It is divided into 7 or 8 cells, each 1.5 cm wide. Each cell contains an anode wire of 50 μm diameter which is supported by plastic hangers, placed every 50 cm along the chamber. The chamber is covered by 4 to 14 cathode pads, which are 50 cm long. The nominal voltage between wires and pads is 1785 V. The mixture of gas in chambers contains of 87 % argon and 13 % CO_2, the drift time is around 100 $\div$ 200 ns.

Figure 13: Specimen of the BAC proportional wire chamber.

3.2 The readout structure of BAC

The basic measurement units in BAC are called wire towers and pad towers (Fig. 12). All wires from 3 or 4 adjacent chambers form so called *xlayer*, then xlayers are connected together over a full calorimeter depth to form a wire tower. On the same rule pad towers are linked (Fig. 14). There are 178 wire towers and 1692 pad towers. The spatial resolution of an energy readout form pads is of the order of 50*50 cm. Moreover, pad towers visible from the interaction point with the same polar angle, form 133 so called strip towers used for trigger purposes.

There are 4 types of readout in BAC:

- *Digital wire readout.* Each chamber has its unique wire signal threshold. If a charged particle ionizes the gas, the charge deposit is compared

with it. If the signal exceeds the threshold, the wire is marked as 'hit' or 'active'. Out of each chamber, 8 bit word is put into FIFO[6] pipeline memory. To reduce ambiguity caused by a long drift time, in comparison to the bunch-crossing frequency, 3 crossings (1 per 96 ns) are read out for each event after a positive trigger decision. Digital wire electronics (or 'hit electronics') serves the purposes of muon tracking trigger.

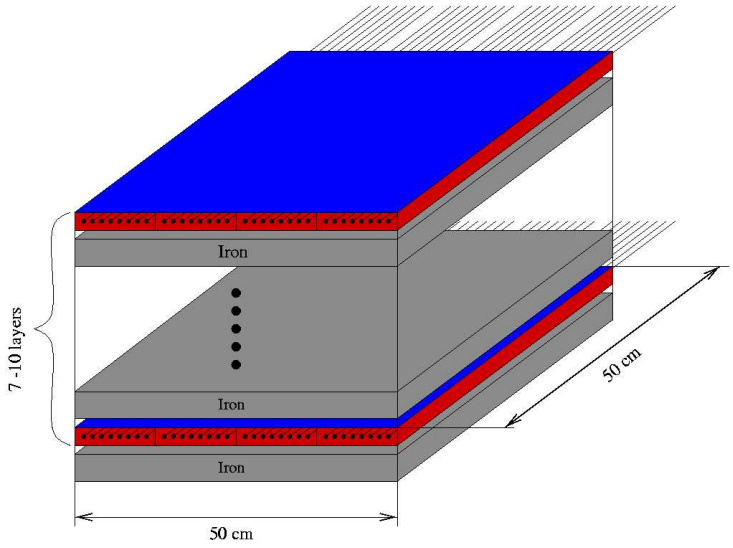

Figure 14: Pad tower scheme

- *Analog wire tower readout.* Energy amplitude signals are preamplified and summed over towers. For each tower the signal is splitted into 2 channels which differ in relative amplification. After passing through the shaper system, the amplitude of the signal is proportional to the charge collected in the chambers. The signals are then digitalized on a Flash ADC board, and stored in the FIFO pipeline memory, where they are waiting for the Global First Level Trigger decision. Because of the hardware constraints, the analog wire pulses are longer then the digital ones, so 12 crossings are read in this case, to properly reconstruct

[6]FIFO pipeline is a chain of memory cells, in which the information proceeds in queue - enters at one end and flows out at another.

off-line the amplitude of the signal.

- *Analog pad tower readout.* As the spatial resolution of readout form pad towers is 10 times higher then the wire hit readout, this part of the system was designed to support tracking of muons. Moreover the energy resolution is comparable to that in the analog wire readout, that is why pads are used both for tracking and energy measurements. Signals go through the same electronic way as in analog wire readout (summing, shaping, digitizing).

- *Analog strip tower readout.* The energy signals from pad towers are summed over the same polar angle to form 133 *strip towers*. Again, signals from strips are shaped and digitized.

3.3 The trigger system of the BAC

Since the beginning of HERA and ZEUS operation in 1992, the energy trigger was implemented in the BAC detector. In 1997 the electronic circuits (HITBOXes) dedicated for muon readout and the muon trigger were mounted in the BAC. Final hardware improvements were undertaken during the 2000-2002 HERA shutdown. During winter and spring 2004, the BAC muon trigger was included in physics runs. Implementing the muon trigger in BAC was very important to fully utilize the upgrade of the HERA luminosity, by increasing overall ZEUS sensitivity to muon final states.

At the trigger level, the BAC is divided into 13 areas: 2 in the Forecap (called EFS and EFN), 2 in the Rearcap (ERS and ERN), 9 in the Barrel (BDRS, BDRN, BDFS, BDFN, BURS, BURN, BUFS, BUFN, BOTT), where following abbreviations denote: E(East), W(West), N(North), F(Foreward), R(Rear), B(Barrel), U(Up), D(Down), BOTT(Bottom).

3.3.1 Energy trigger stream

As described in section 3.2 energy deposits are measured by wire and strip towers and digitized. Data is stored in pipeline memories, when the local first level trigger boards evaluate the decision. It contains 16 bits of total energy (from wire towers), 16 bits of transverse energy (from strip towers), and 32 bits for the value and the geometrical location of two highest energy deposits in BAC. All this information is sent to the Global First Level Trigger.

3.3.2 Muon trigger stream

The BAC muon trigger uses data from the position readout. Since it has to respond in only $2.5\mu s$, the first level trigger is fully hardware implemented. The HITBOX module calculates the sum of 'active' xlayers (up to 10) and 'active' chambers (up to 40) for each wire tower. The chamber is 'active' or 'fired' if at least one wire was hit by a propagating particle, and the xlayer is 'active' or 'fired' if at least one chamber is active. These sums (6 bits for chambers sum, and 4 bits for xlayers sum) form an address in the programmable Lookup Table Memory (LTM). Output of this memory has 2 bits, marked as X and Y.

The algorithm of muon trigger (Fig. 15) is meant to distinguish muons, hadrons, and noise signals, and give positive decisions only in case of muon events. It is based on an observation that hadron cascades should activate more chambers then xlayers, while a muon track should give both numbers approximately equal. So, if the number of active chambers is approximately equal to the number of active xlayers, and both these numbers are greater then the threshold values, the particle is considered as a muon.

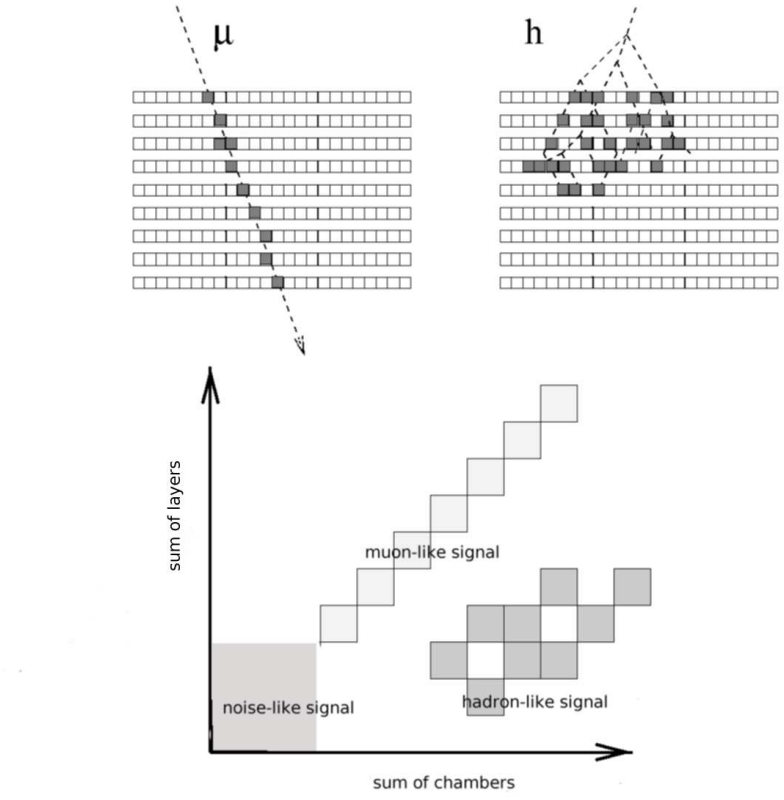

Figure 15: Behavior of muons(μ) and hadrons(h) in BAC wire towers and 2-dimensional visualization of Lookup Table Memory

The LTM memory plays a crucial role in the algorithm. It has 1024 cells, so it is addressed with 10 bits (6 bits for chamber sum and 4 bits for xlayer sum), each cell contains 2 predefined bits, called X and Y. The filling pattern of the LTM memory, with sums of xlayers and chambers as

axes, forms a rectangle with a 'diagonal' marked out (Fig 15). The rectangle defines which signals are legal - greater then possible electronics noises, and with maximum of 10 xlayers and 40 chambers. The 'diagonal' is defined to distinguish muons from hadrons. If $\sum xlayers \approx \sum chambers$, X bit is set to 1, Y is set to 0. If $\sum xlayers < \sum chambers$, then X = 0, Y = 1. And if both sums are comparable to noises (values up to 3-4 layers and chambers), then X = Y = 0.

When X and Y bits are computed, the information is further processed on the level of areas in BAC. The computed X and Y bits are sent to XY-Receiver (XYREC) board, that produces arithmetic sum of all X bits ($\sum X$) and stores Y bits from each tower. These values are afterwards sent to the Logic of the Trigger (LT) board. In the simplest algorithm, $\sum X$ is compared with the programd threshold level - Th1(LT) and if $\sum X \geqq Th1(LT)$ the LT board sets b0 (muon in area) bit to 1, otherwise, b0 is set to 0. The LT board offers much wider capabilities, as both trigger streams (energy and tracking) are processed there. The muon hit information can be correlated with strip or wire tower energies. On the output of muon trigger, each LT board has 3 additional bits: b1, b2, b3 which are meant to mark vertex, cosmic, and halo muons.

Finally on the level of the whole BAC, muon hit information is processed on BT and BM boards, and formed as final 16-bits word, sent to the Global First Level Trigger. So far (March, 2004) 13 b0 bits pattern, marking if there was a muon in a given area, is sent to GFLT.

In the current configuration, when the BAC trigger system receives an 'accept' signal from GFLT, it starts the local Second Level Trigger procedure. The program, written in *occam2*, and processed on the transputer network, reads the 'hit data' and sends the number and addresses of towers that detected a muon. This procedure allows to locate a muon signal with a wire tower resolution that improves a spatial resolution by a factor of 12 comparing to the First Level Trigger (162 wire towers on the SLT level, 13 areas on the FLT areas).

4 BAC trigger simulation and reconstruction

4.1 ZEUS Monte Carlo Chain

The aim of the ZEUS Monte Carlo Chain is to simulate the entire detector, starting from the *ep* interactions, to the detector response and the reconstructed physical quantities. It consists of 4 main programs:

- *AMADEUS*. The AMADEUS is a package of Monte Carlo event generators of physical processes. Among others, it consists of following programs: PYTHIA (QCD simulation), HERWIG (Hadron Emission Reactions With Interfering Gluons), RAPGAP (for Deep Inelastic Scattering and diffraction), DIPSI (for Elastic Vector Meson Production), or LEPTO (for DIS). At this stage the user can select the interesting class of processes for further studies. However AMADEUS doesn't offer complete variety of all processes observed in the detector, because it doesn't simulate background sources like beam-gas, cosmic particles or proton beam halo-muon events.

- *MOZART*. The MOZART (Monte Carlo for ZEUS Analysis, Reconstruction and Trigger) package is a simulation of the ZEUS detector, based on GEANT package. The GEANT program describes the passage of elementary particles through the matter so in High Energy Physics it is used for simulation of detector response. The MOZART code includes ZEUS components geometry and technical properties. As the input it requires events from the Monte Carlo event generator, and on the output it produces the standard ZEUS ADAMO database tables containing simulated raw data in the format identical to the real data collected with the detector. In that way, at all subsequent stages of data analysis, the same software can be used for data and Monte Carlo events. Such an approach reduces systematic uncertainties related to the reconstruction software.

- *CZAR/ZGANA*. The CZAR/ZGANA is a package of local and global trigger simulations, using the output data of MOZART. It includes trigger algorithms specific for the components taking part in the trig-

ger system. Given the ZEUS components responses from MOZART, CZAR/ZGANA is able to work out the final decision, with no efficiency losses caused by hardware failures. Since as input CZAR/ZGANA uses raw data ADAMO tables, it can also work as an off-line reconstruction of real trigger decisions (but only for components that write their trigger data to DST after positive trigger decision).

- *ZEPHYR.* The ZEPHYR package is the final step in the whole MC (real data as well) chain for ZEUS. It is a collection of reconstruction algorithms specialized in computing physical quantities like energy deposits, momenta, tracks or particle identification.

4.2 Implementation of the BAC muon trigger for the CZAR/ZGANA package

As stated above, the main motivation for the work described in this thesis, was creating the BAC muon trigger simulation, which was a part of the upgrade of the BAC detector. In addition to energy trigger, that was already implemented in the CZAR/ZGANA prior simulation, the new muon trigger code is described in the following.

The whole CZAR/ZGANA code is written in Fortran, supported with the EAZE environment, which includes the ZEUS and CERN libraries and allows the programmer for an easy access to any data taken by the detector or generated with MC event simulation. The main BAC trigger routine is *FLSBAC* that communicates BAC trigger decision bits to GFLT module. It reads the Control Cards - the file that allows the user to set selected functions of the simulation (i.e. XY memory fillings or LT boards thresholds values) and initializes all global variables. Addresses of XY LTM memory filling parameters are translated from hardware terms (board/channel oriented) to *hex-indices*[7], and LTM memories (1 per wire tower) are filled. Then *BACFLT* routine is called, that computes the BAC decision bits for each event.

[7]The *hex-index* is the detector oriented tower identifier and contains such informations as: the tower type, the BAC unit number, area number, *cx,cy* - tower position on the 2-dimensional plane or finally the layer number in a given tower.

The *BACFLT* routine consists of a chain of subroutines, out of which vital for muon trigger are:

- BACGET - it reads XXXLRD ADAMO table, that contains hit patterns from all fired wires in BAC chambers. Each record in XXXLRD contains so called hex-index (32 bits word defining the position of each BAC tower/xlayer and readout type) and 32 bits of hit pattern for every xlayer. Raw data contain 3 time samples for each active xlayer, MC data just 1, as the charge drift is not simulated. In case of raw data, the so called 'right-hand OR' operation is performed, that allows to follow signal evolution in time. In parallel, the data from XXPSRD table is read (only in case of real data). It stores the pattern of all X and Y bits, recorded on-line by the trigger electronics. Comparison of off-line reconstructed trigger decisions with on-line written values (XXPSRD table) allows to monitor the trigger and readout quality performing the cross-check.

- BACSETXY - computes sums of fired chambers and xlayers for all active wire towers. Next, 10 bits address (6 bits of chamber sum and 4 bits of xlayer sum) points at LTM memory cell from which X and Y bits are read, X = 1 is set if there was a muon, X = Y = 0 if the signal is compatible with noise. Having LTM filling parameters available in Control Cards, allows to test the system response against various fillings easily. The algorithm of filling LTM XY memories is available in [22].

- BACXYREC - sums X bits from each area and passes them to LT boards, passes Y bits to WTT boards.

- BACDLT - compares if X bits sum from each area is equal or higher then the predefined ones. If so, then b0 bit is set to 1 for this area, and passed further.

- BACDGL - builds the final muon trigger decision word, which consists of 13 muon bits from each area and 2 additional bits left for future usage.

The final BAC muon trigger simulation output variables, available in FLSBAC common block, are:

- b0(area) - 13 BAC FLT decision bits (1 per area)
- CountX(area,tower), CountY(area,tower) - 162 X and 162 Y decision bits (BAC SLT). They are computed on the basis of xlayers and chambers sums, after 'right-hand OR' operation. In case of raw data this sets X and Y bits to 1, even if they were seen only in one (out of three) time sample (i.e. time evolution is not simulated and only 'time OR-ed' values are compared).

5 Efficiency of the BAC trigger

The current chapter presents Monte Carlo studies based on the BACFLT CZAR/ZGANA routine. It is based on decay of the heavy vector mesons $(\Upsilon, \Psi', J/\Psi)$, beauty quark decay and the elastic Bethe-Heitler process with muons in the final state. All the simulations presented here and in appendices are based on LTM XY memory filling (dedicated to recognize muon signals - more detailed description in 3.3.2) given in [24].

5.1 Efficiency of the BAC muon trigger simulation algorithm

The algorithm used for the present Monte Carlo studies allows to estimate the ratio of triggered muons (and any other particles giving trigger signals) and muon tracks in BAC. The MOZART simulation file of the given process in ZEUS detector consitutes the input file for the trigger simulation. Subsequently the BACFLT ZGANA routine computes the BAC muon trigger decision for each wire tower allowing also to see how the trigger decision is evaluated in various regions of the detector.

The trigger efficiency has been studied as a function of the muon momentum. The algorithm uses CTD and CAL ZEPHYR reconstruction routines to determine the track momenta and their position in the CAL. The XCrosLay routine from the BAC ZEPHYR reconstruction program is used to extrapolate the muon trajectory to the BAC tower which the muon coming out from CAL should hit. However it might happen that the the XCrosLay routine and BAC hit positions differ with the tower index cy[8] by 1. That is the reason why the triggered - track matching algorithm assumes that the cy index from XCrosLay should be equal to the values: $(cy-1)$, cy or $(cy+1)$ of the index in the BACFLT ZGANA triggered record. Finally the risk of matching two adjacent triggered towers to just one track is supressed [9].

[8] cx and cy indices describe the position of a BAC, on the 2-dimensional mapping (unfolding the barrel) of the detector to a plane.

[9] If X bits of two adjacent towers are set to 1, only one muon trigger signal is taken into analysis.

Mnemonic and numerical indices of the areas of the BAC are given in Section 3.3[10].

5.2 Results of the BAC muon trigger efficiency simulation

5.2.1 Υ decay sample

Area	Description	$\mathcal{E}_\Upsilon$
0	BDRS	0.880 ± 0.010
1	BDRN	0.930 ± 0.008
2	BDFS	0.919 ± 0.008
3	BDFN	0.908 ± 0.008
4	BURS	0.882 ± 0.008
5	BURN	0.932 ± 0.006
6	BUFS	0.910 ± 0.006
7	BUFN	0.921 ± 0.006
8	ERS	0.823 ± 0.001
9	ERN	0.822 ± 0.001
10	EFS	0.929 ± 0.005
11	EFN	0.910 ± 0.006
12	BOTT	0.896 ± 0.007

Table 2: MC muon trigger efficiencies for individual BAC areas obtained with Υ sample

The sample used for this part of efficiency studies was 20000 events of $\Upsilon \rightarrow \mu + \mu-$ decay generated with DIFFVM [31], with the kinematic variables chosen as follows:

$$4.0 \geq Q^2 \geq 0.0 \; [GeV^2] \tag{22}$$

$$318.4 \geq W \geq 11.4 \; [GeV] \tag{23}$$

$$0.5 \geq y \geq 0.005. \tag{24}$$

[10]Areas 0-7 are the Barrel without Bottom part, Areas 8-9 are in the Rearcap, Areas 10-11 are in the Forecap, and area 12 is the Bottom part of the Barrel.

Fig. 16 depicts the total efficiency of the BAC muon trigger as a function of the muon momentum with the Υ sample. The similar plots for each Area (Fig. 21 - 33), are presented in Section 7.1, as well as numbers of positive trigger decisions of each BAC tower (Fig.34-36).

Discussion of results. The values of efficiency for each area are summarized in Table 2. The horizontal straight line fit was done for the range of the muon momentum from 2.5 to 13 GeV yielding the muon trigger efficiency of

$$\mathcal{E}_\Upsilon = 0.892 \pm 0.002. \tag{25}$$

The top plot in Fig. 16 shows histograms with all muon tracks that left CTD and muons which produced a positive trigger decision in the BAC, matched together using the algorithm described in section 5.1. The bottom plot results from dividing the histograms from the upper plot. Thus the quoted efficiency refers to the muons with momentum sufficiently large to let the muon rech the BAC. The position of the maximum on the upper plot at about 4.5 GeV, in view of the Υ mass indicates that the mesons are produced with predominantly low momenta.

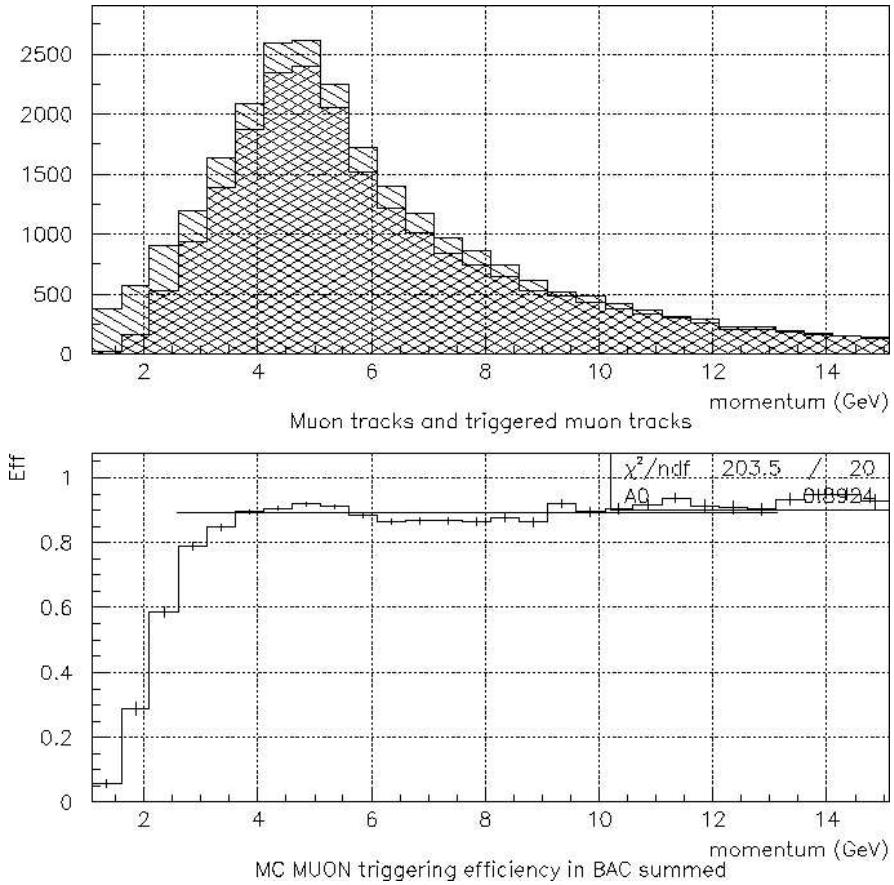

Figure 16: Plots for the Υ sample. Upper: muon tracks ($\backslash\backslash$) and triggers matched to them ($//$). Lower: MC muon trigger efficiency results for the whole BAC.

5.2.2 Beauty quark decay sample

The sample used for this part of efficiency studies was 20000 events of beauty quark decays. The sample was generated by the RAPGAP [32] program, with the kinematic variables chosen as follows:

$$1.0 \geq x \geq 0.0 \tag{26}$$

$$10.0^5 \geq Q^2 \geq 1.0\ [GeV^2] \tag{27}$$

$$W \geq 5\ [GeV] \tag{28}$$

$$1.0 \geq y \geq 5.0 \cdot 10^{-3}. \tag{29}$$

Fig. 17 depicts the total efficiency of the BAC muon trigger as a function of the muon momentum with the beauty quark sample. The similar plots of each Area (Fig. 37 - 49), are presented in Section 7.2, as well as numbers of positive trigger decisions of each BAC tower (Fig. 50 - 52).

Area	Description	$\mathcal{E}_{beauty}$
0	BDRS	0.56 ± 0.08
1	BDRN	0.63 ± 0.06
2	BDFS	0.59 ± 0.05
3	BDFN	0.59 ± 0.07
4	BURS	0.68 ± 0.05
5	BURN	0.69 ± 0.05
6	BUFS	0.70 ± 0.04
7	BUFN	0.54 ± 0.04
8	ERS	0.37 ± 0.03
9	ERN	0.46 ± 0.04
10	EFS	0.45 ± 0.02
11	EFN	0.46 ± 0.02
12	BOTT	0.79 ± 0.04

Table 3: MC muon trigger efficiencies for individual BAC areas obtained with beauty quarks sample

Discussion of results. The values of efficiency for each Area are summarized in Table 3. The horizontal straight line fit was done for the range of the

muon momentum from 2.5 to 13 GeV yielding the muon trigger efficiency of

$$\mathcal{E}_{beauty} = 0.51 \pm 0.01. \tag{30}$$

What requires a comment is much lower trigger efficiency then in other processes (for example Υ decay). Muons from beauty decays are ofted contained in hadronic jets, and some of them have almost parrarel trajectories (when produced in the same jet). Due to the algorithm used in this analysis, when 2 muons get to the same BAC wire tower, they give only 1 trigger signal. Moreover, a significant proton-remnant hadron activity perturbs trigger decisions when a hadron and a muon hit the same BAC wire tower. That is why the value of $\mathcal{E}_{beauty} = 0.51 \pm 0.01$ efficiency may be concerned as a lower limit on BAC capabilities of triggering muons from beauty quark decay.

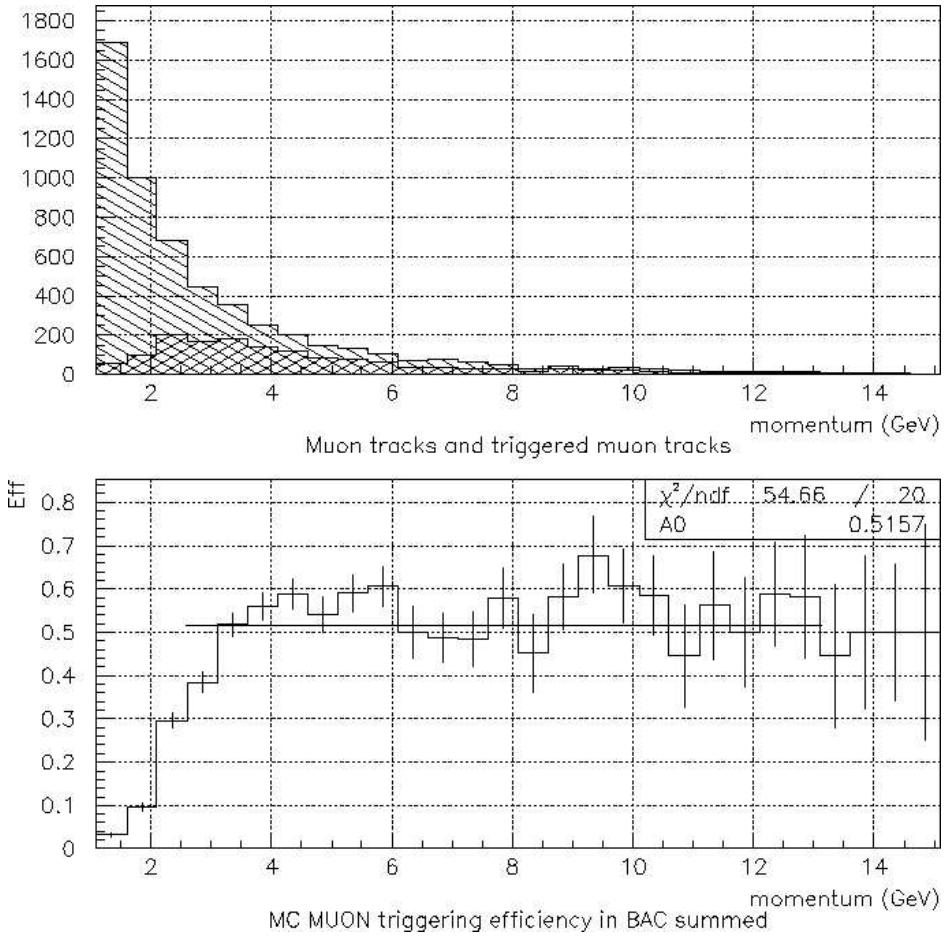

Figure 17: Plots for the beauty quark sample. Upper: muon tracks (\\) and triggers matched to them (//). Lower: MC muon trigger efficiency results for the whole BAC.

5.2.3 Ψ' sample

The sample used for this part of efficiency studies was 50000 events of Ψ' vector mesons (produced in pe^+ collisions) decay. The sample was generated with the DIFFVM [31] program.

Fig. 18 shows the total efficiency of the BAC muon trigger as a function of the muon momentum with the Ψ' sample. The similar plots for each Area (Fig. 53 - 65) are presented in Section 7.3, along with numbers of positive trigger decisions of each BAC tower (Fig. 66 - 68).

Area	Description	$\mathcal{E}_{\Psi'}$
0	BDRS	0.776 ± 0.014
1	BDRN	0.796 ± 0.013
2	BDFS	0.735 ± 0.026
3	BDFN	0.677 ± 0.028
4	BURS	0.752 ± 0.010
5	BURN	0.818 ± 0.009
6	BUFS	0.761 ± 0.020
7	BUFN	0.734 ± 0.020
8	ERS	0.741 ± 0.003
9	ERN	0.788 ± 0.004
10	EFS	0.751 ± 0.016
11	EFN	0.750 ± 0.015
12	BOTT	0.681 ± 0.002

Table 4: MC muon trigger efficiencies for individual BAC areas obtained with the Ψ' sample

Discussion of results. The values of efficiency for each Area are summarized in Table 4. The horizontal straight line fit was done for the range of the muon momentum from 2.5 to 13 GeV, yielding the muon trigger efficiency of

$$\mathcal{E}_{\Psi'} = 0.757 \pm 0.002. \tag{31}$$

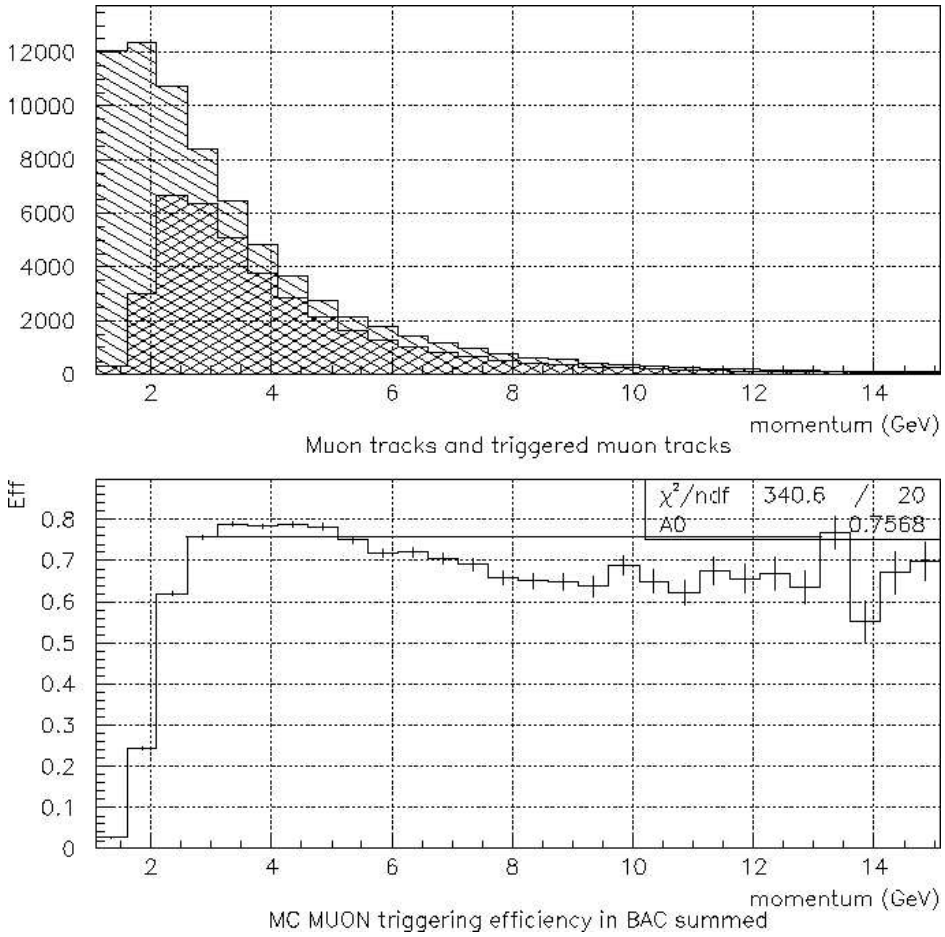

Figure 18: Plots for the Ψ' sample. Upper: muon tracks ($\backslash\backslash$) and triggers matched to them ($//$). Lower: MC muon trigger efficiency results for the whole BAC.

5.2.4 J/Ψ sample

The sample used for this part of efficiency studies was 80000 events of J/Ψ vector mesons (produced in pe^+ collisions) decay. The sample was generated by HERACLES [33] program. The kinematic region was as follows:

$$Q^2 \geq 1.0\ [GeV^2] \tag{32}$$

$$260 \geq W \geq 10\ [GeV] \tag{33}$$

$$0.2 \geq x \geq 0. \tag{34}$$

Fig. 19 shows the total efficiency of the BAC muon trigger as a function of the muon momentum with the J/Ψ sample. The similar plots for each Area (Fig. 69 - 81) are given in Section 7.3 as well as numbers of positive trigger decisions of each BAC tower (Fig. 82 - 84).

Area	Description	$\mathcal{E}_{J/\Psi}$
0	BDRS	0.730 ± 0.014
1	BDRN	0.797 ± 0.012
2	BDFS	0.702 ± 0.015
3	BDFN	0.721 ± 0.015
4	BURS	0.757 ± 0.010
5	BURN	0.792 ± 0.010
6	BUFS	0.743 ± 0.012
7	BUFN	0.745 ± 0.012
8	ERS	0.740 ± 0.004
9	ERN	0.786 ± 0.004
10	EFS	0.875 ± 0.004
11	EFN	0.877 ± 0.004
12	BOTT	0.709 ± 0.018

Table 5: MC muon trigger efficiencies for individual BAC areas obtained with the J/Ψ sample

Discussion of results. The values of efficiency for each Area are summarized in Table 5. The horizontal straight line fit was done for momenta from

2.5 to 13 GeV yielding the muon trigger efficiency of:

$$\mathcal{E}_{J/\Psi} = 0.773 \pm 0.002. \tag{35}$$

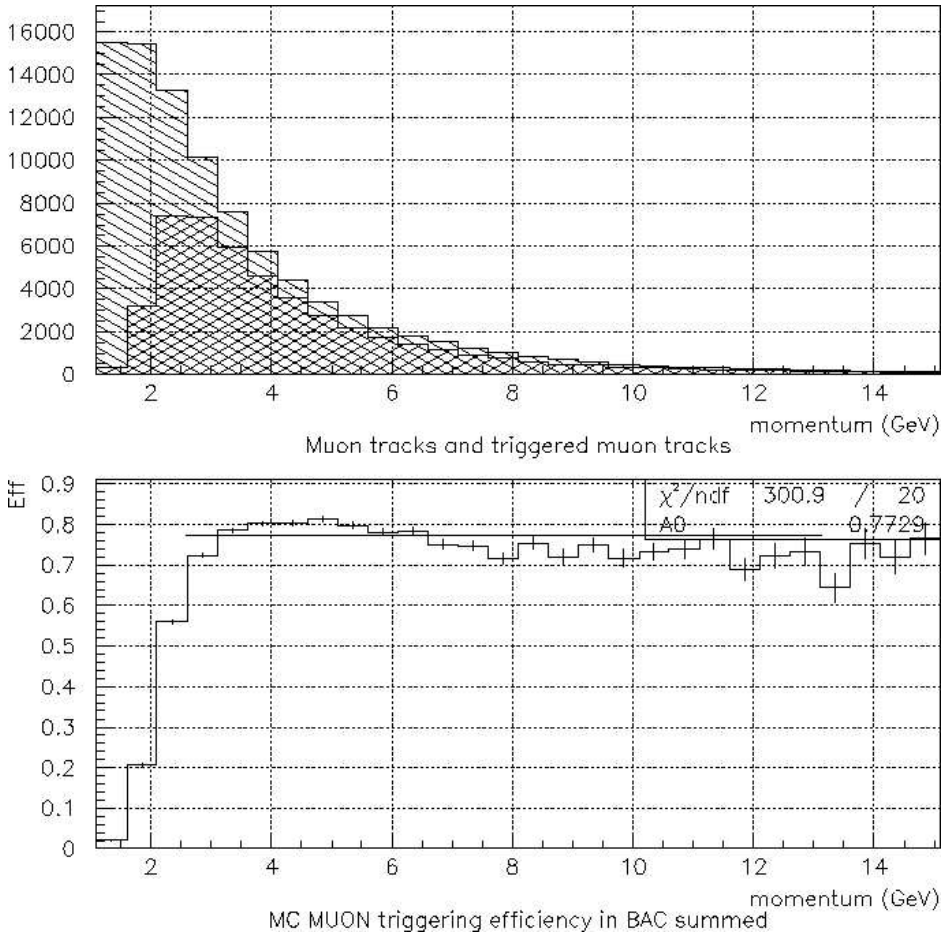

Figure 19: Plots for the J/Ψ sample. Upper: muon tracks ($\backslash\backslash$) and triggers matched to them ($//$). Lower: MC muon trigger efficiency results for the whole BAC.

5.2.5 Elastic Bethe-Heitler process sample

The sample used for this part of efficiency studies was 140000 events of the elastic $e + p \rightarrow el^+l^-p$ Bethe-Heitler process with 2 muons in the final state. The sample was generated by GRAPE [34] program.The kinematic region was as follows:

$$Q^2 \ \geq \ 1.0 \ [GeV^2] \tag{36}$$

$$M_{inv} \ \geq \ 1.5 \ [GeV]. \tag{37}$$

Fig. 20 shows the total efficiency of the BAC muon trigger as a function of the muon momentum with the Bethe-Heitler sample. The similar plots for each Area (Fig. 85 - 97) are presented in Section 7.5 along with numbers of positive trigger decisions of each BAC tower (Fig. 98 - 99).

Area	Description	$\mathcal{E}_{Bethe-Heitler}$
0	BDRS	0.795 ± 0.009
1	BDRN	0.812 ± 0.008
2	BDFS	0.769 ± 0.009
3	BDFN	0.767 ± 0.009
4	BURS	0.797 ± 0.006
5	BURN	0.833 ± 0.006
6	BUFS	0.771 ± 0.007
7	BUFN	0.763 ± 0.008
8	ERS	0.718 ± 0.003
9	ERN	0.777 ± 0.003
10	EFS	0.813 ± 0.004
11	EFN	0.825 ± 0.004
12	BOTT	0.773 ± 0.007

Table 6: MC muon trigger efficiencies for individual BAC areas obtained with the elastic Bethe-Heitler sample.

Discussion of results. The values of efficiency for each Area are summarized in Table 6. The horizontal straight line fit was done for momenta

from 2.5 to 13 GeV. The muon trigger efficiency obtained with the elastic Bethe-Heitler sample was

$$\mathcal{E}_{Bethe-Heitler} = 0.769 \pm 0.001. \tag{38}$$

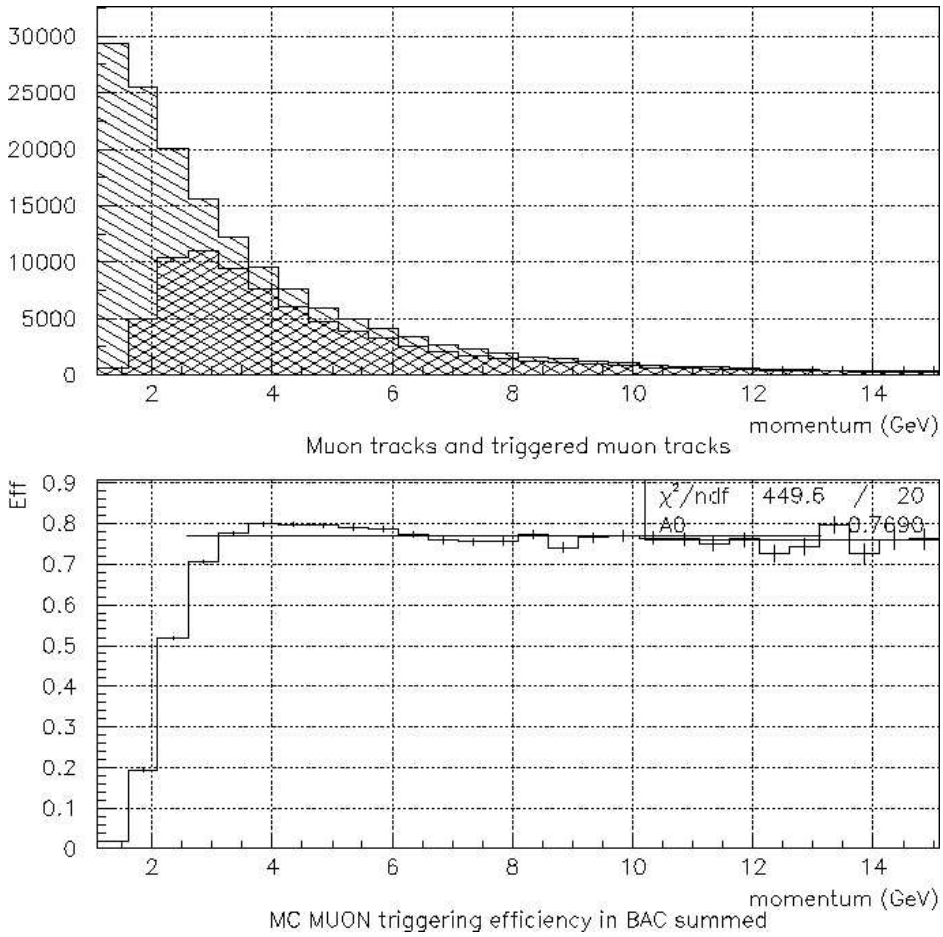

Figure 20: Plots for the elastic Bethe-Heitler sample. Upper: muon tracks (\\) and triggers matched to them (//). Lower: MC muon trigger efficiency results for the whole BAC.

6 Summary

The currently implemented BAC muon trigger is a promising system to enable more detailed studies of ep interactions with muons in the final state in the ZEUS experiment, like heavy quarks decays or exotic phenomena. The $BACFLT$ set of routines for $CZAR/ZGANA$ trigger simulation package allows to test the BAC trigger response test for any $ep \to X + N\mu$ process with Monte Carlo sample.

The BAC muon trigger efficiency results, presented in this thesis show that with no hardware failures, the lower limits for the BAC trigger efficiency are:

$$\mathcal{E}_{\Upsilon} = 0.892 \pm 0.002, \tag{39}$$

$$\mathcal{E}_{beauty} = 0.51 \pm 0.01, \tag{40}$$

$$\mathcal{E}_{\Psi'} = 0.757 \pm 0.002, \tag{41}$$

$$\mathcal{E}_{J/\Psi} = 0.769 \pm 0.001, \tag{42}$$

$$\mathcal{E}_{Bethe-Heitler} = 0.769 \pm 0.001, \tag{43}$$

for the Υ, beauty quark, Ψ', J/Ψ and elastic Bethe-Heitler process samples, respectivelly.

Comparing to the trigger efficiency of the BRMuon chambers - another muon detector in ZEUS, which is estimated to be of $\mathcal{O}(0.7)$, the presented results prove that the BAC muon triggering system can significantly improve the ZEUS trigger capabilities.

7 Appendix: More simulation results

The details of the studies presented in Chapter 5 are given in the following. The efficiency plots (e.g. Fig. 21) are similar to presented previously, and show information for each BAC Area. Moreover, number of positive trigger decisions for each BAC tower (e.g. Fig. 34) is presented. Since these are histograms showing number of positive trigger decisions given by each BAC wire tower in the chosen Area, only the relative bin heights are important, not the number of counts. In Areas 8 and 9 (Forecap) every second bin is empty, out of hardware configuration (the trigger signals from two adjacent towers are combined before they flow into a HITBOX, with exception to towers 13 and 14).

7.1 Υ sample

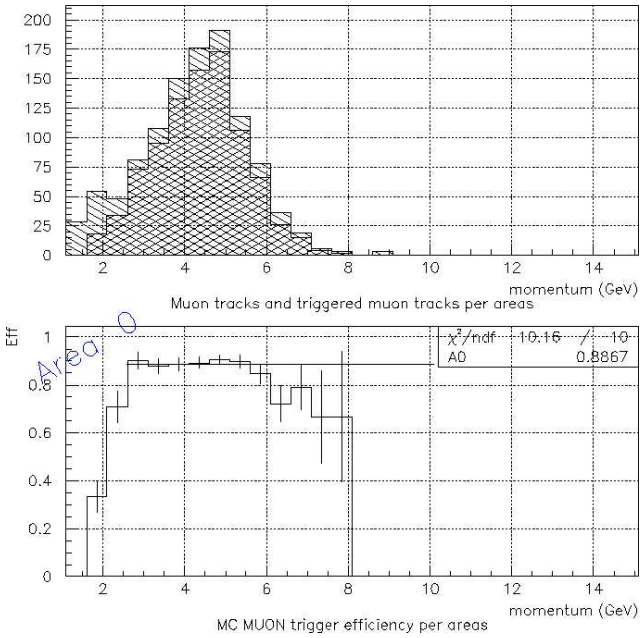

Figure 21: MC muon trigger efficiency results for Area 0 with the Υ sample

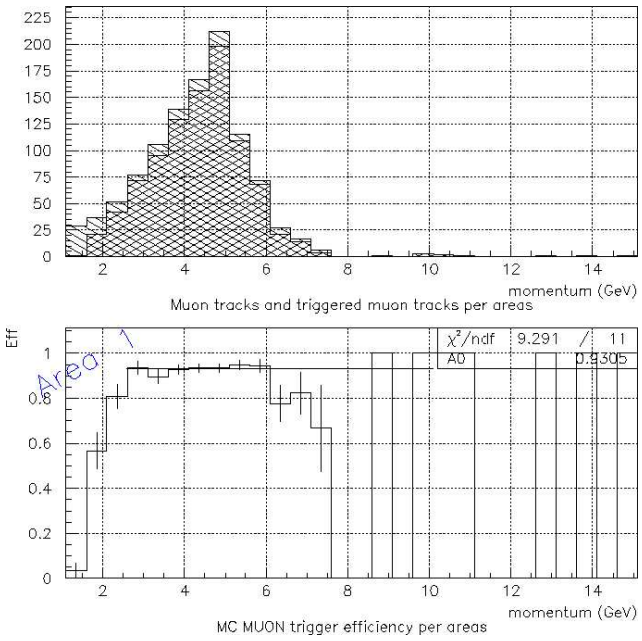

Figure 22: MC muon trigger efficiency results for Area 1 with the Υ sample

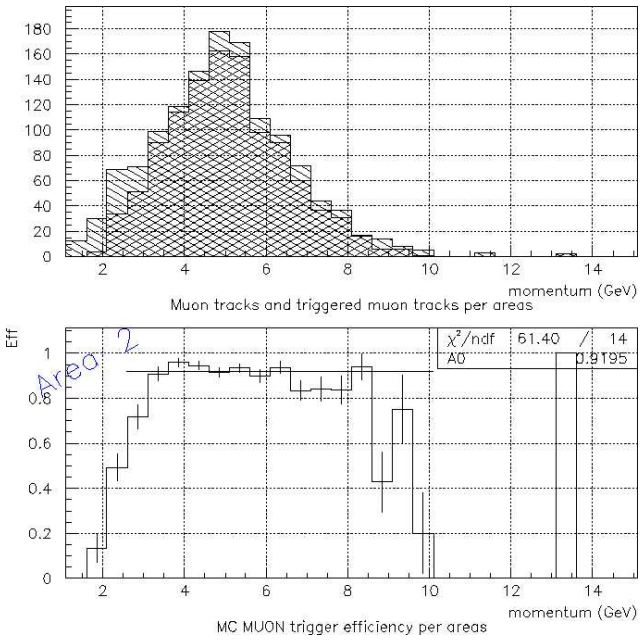

Figure 23: MC muon trigger efficiency results for Area 2 with the Υ sample

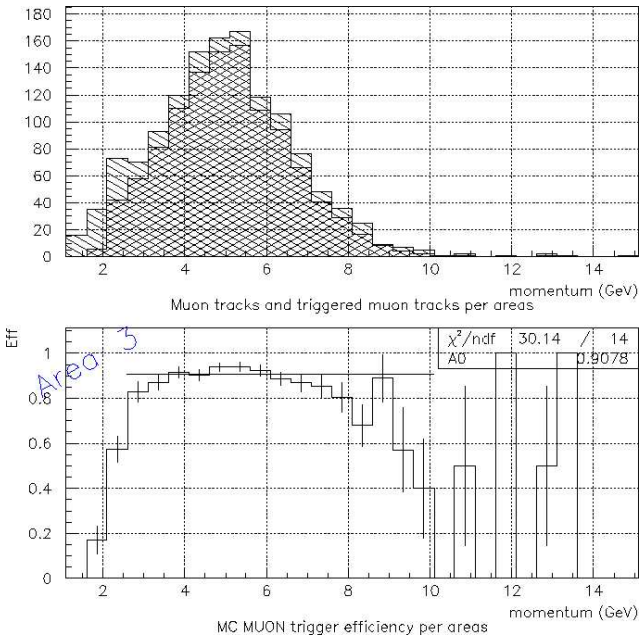

Figure 24: MC muon trigger efficiency results for Area 3 with the Υ sample

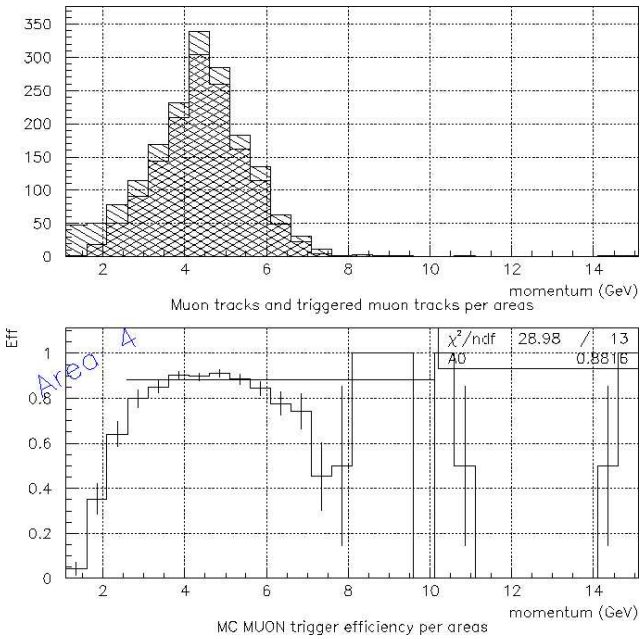

Figure 25: MC muon trigger efficiency results for Area 4 with the Υ sample

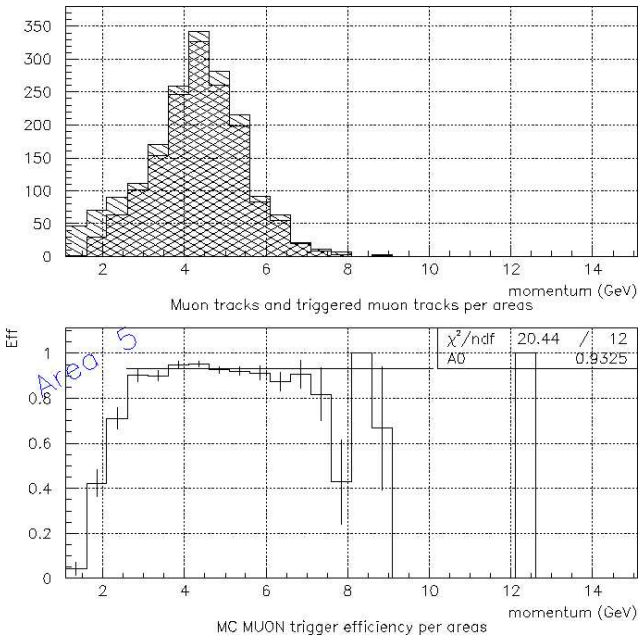

Figure 26: MC muon trigger efficiency results for Area 5 with the Υ sample

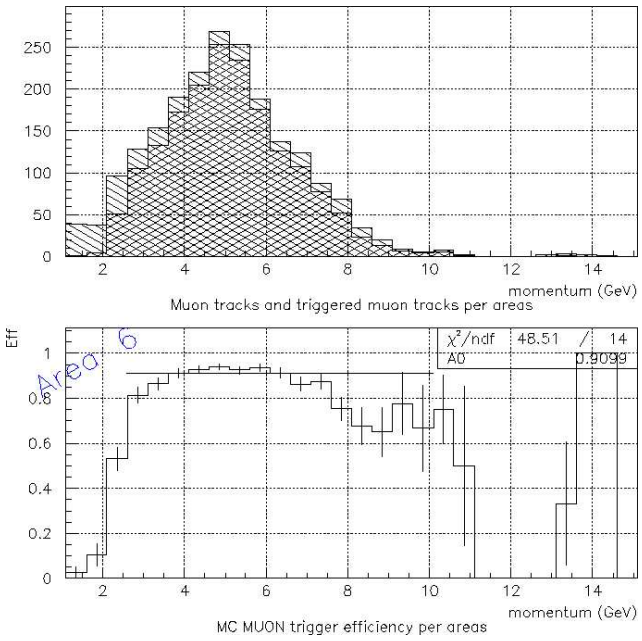

Figure 27: MC muon trigger efficiency results for Area 6 with the Υ sample

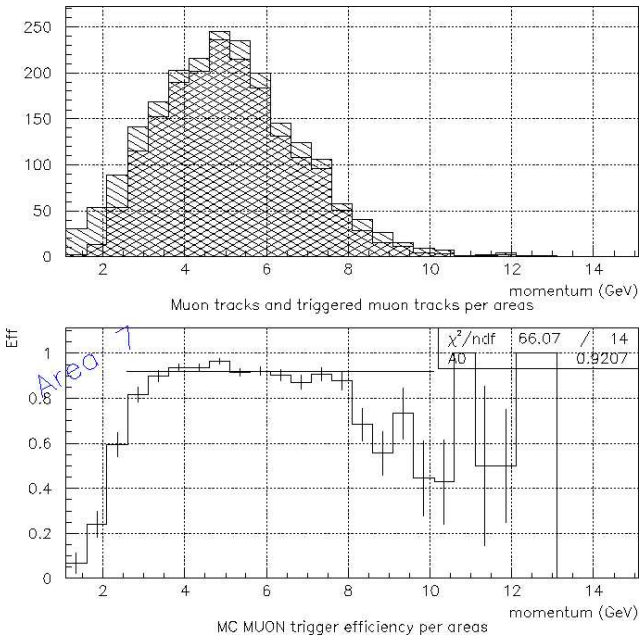

Figure 28: MC muon trigger efficiency results for Area 7 with the Υ sample

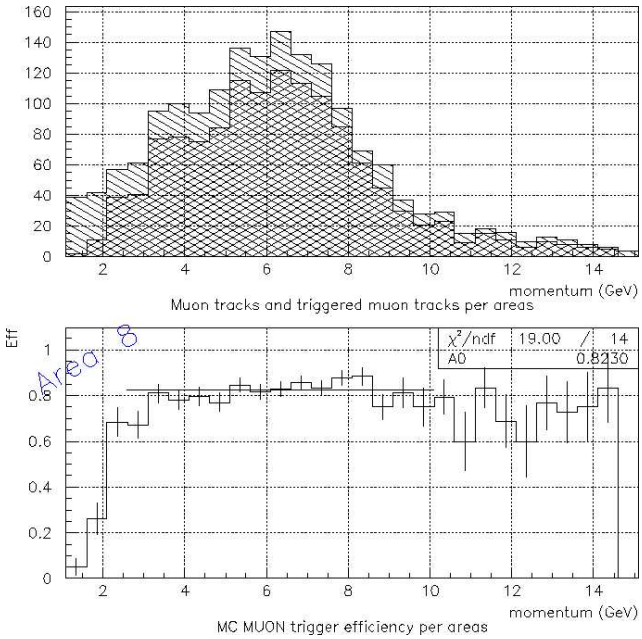

Figure 29: MC muon trigger efficiency results for Area 8 with the Υ sample

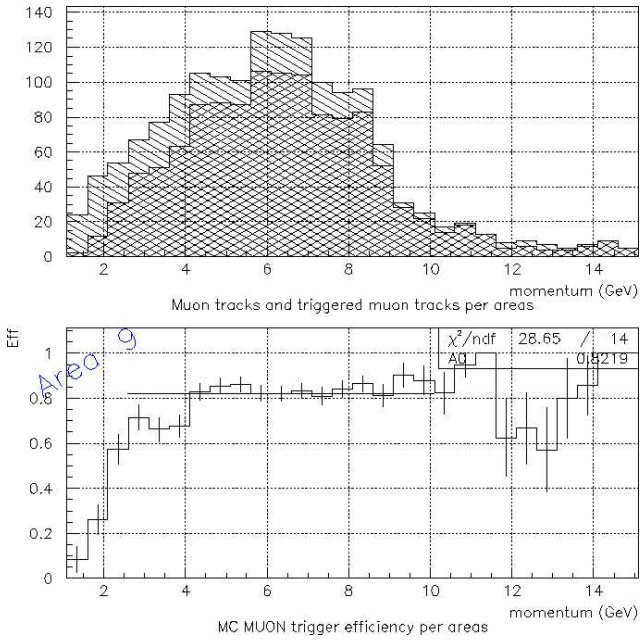

Figure 30: MC muon trigger efficiency results for Area 9 with the ϒ sample

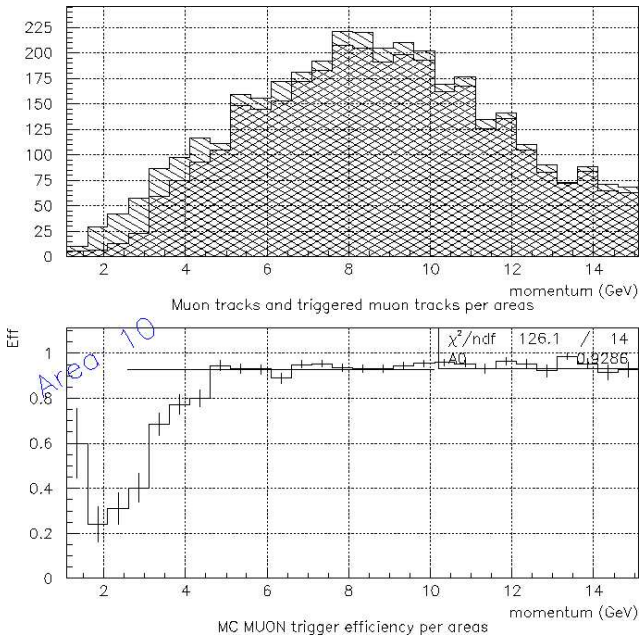

Figure 31: MC muon trigger efficiency results for Area 10 with the ϒ sample

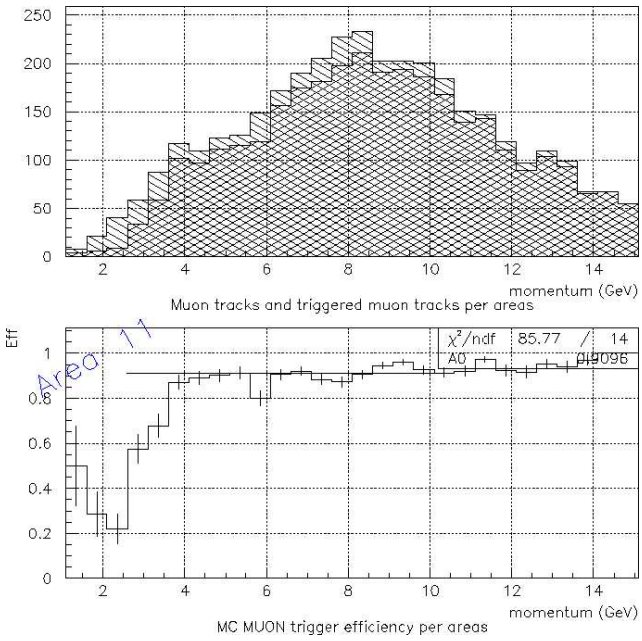

Figure 32: MC muon trigger efficiency results for Area 11 with the Υ sample

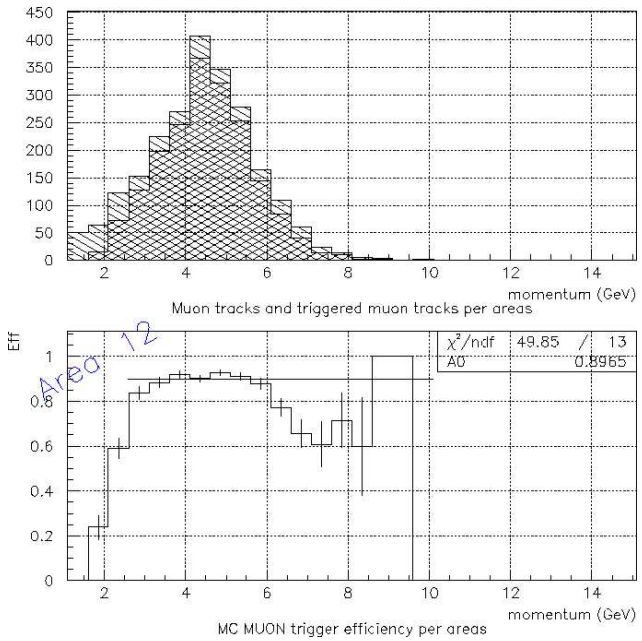

Figure 33: MC muon trigger efficiency results for Area 12 with the Υ sample

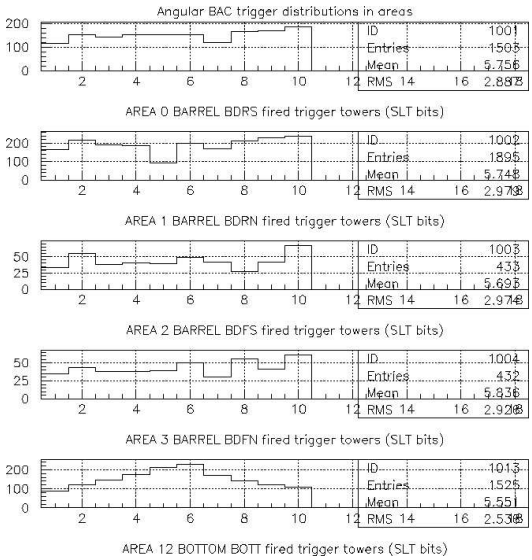

Figure 34: MC muon trigger angular distributions for Areas 0-4 and 12 with the Υ sample

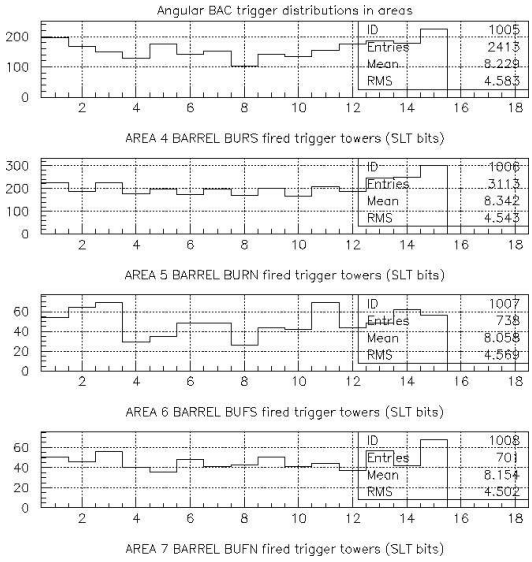

Figure 35: MC muon trigger angular distributions for Areas 4-7 with the Υ sample

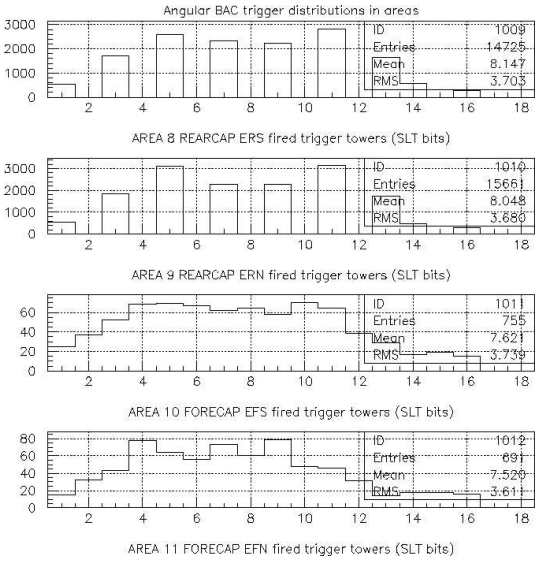

Figure 36: MC muon trigger angular distributions for Areas 8-11 with the Υ sample

7.2 Beauty quark sample

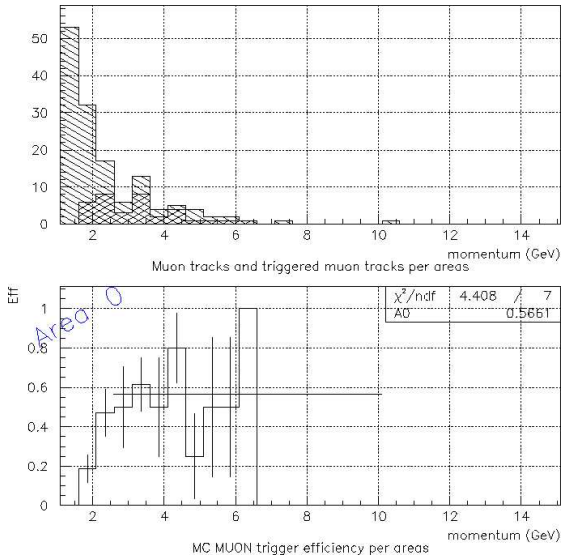

Figure 37: MC muon trigger efficiency results for BAC area 0 with the beauty quark sample

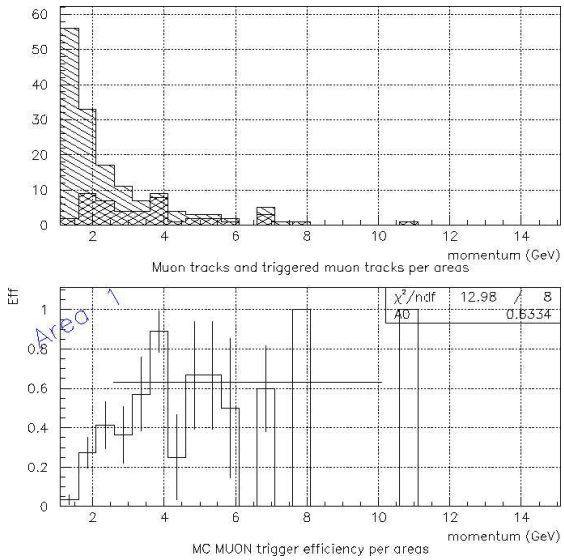

Figure 38: MC muon trigger efficiency results for BAC area 1 with the beauty quark sample

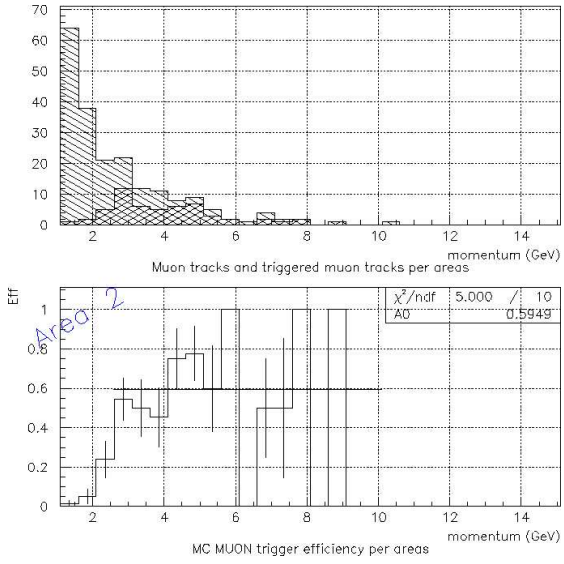

Figure 39: MC muon trigger efficiency results for BAC area 2 with the beauty quark sample

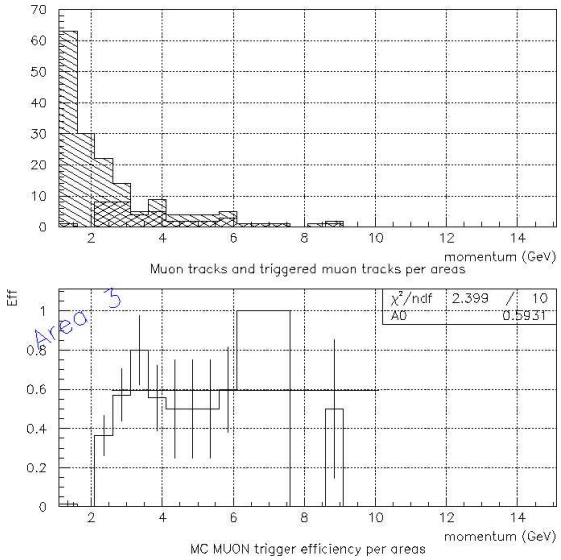

Figure 40: MC muon trigger efficiency results for BAC area 3 with the beauty quark sample

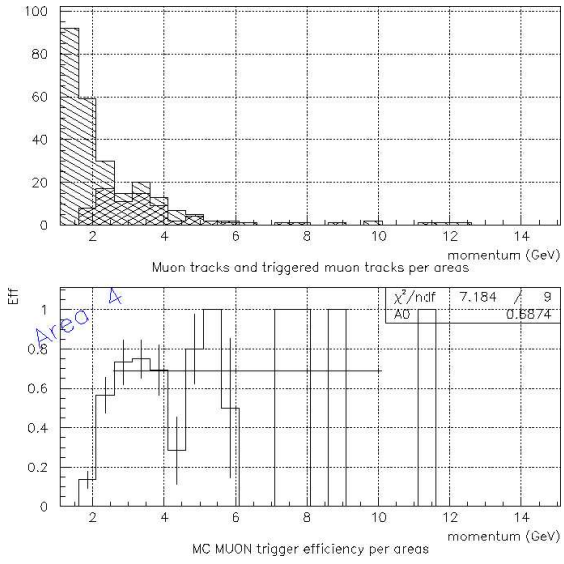

Figure 41: MC muon trigger efficiency results for BAC area 4 with the beauty quark sample

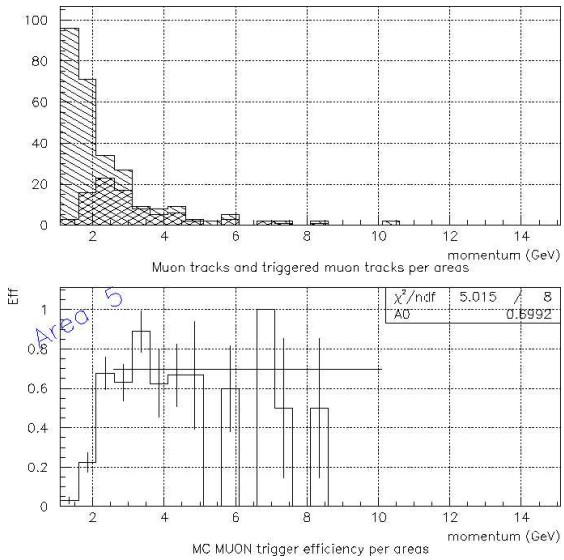

Figure 42: MC muon trigger efficiency results for BAC area 5 with the beauty quark sample

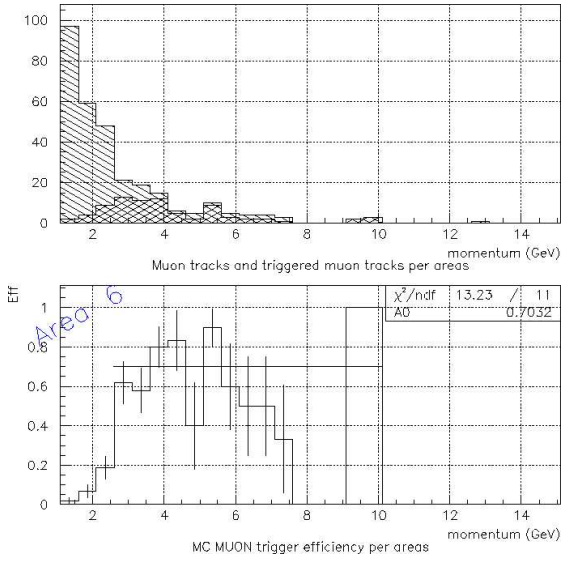

Figure 43: MC muon trigger efficiency results for BAC area 6 with the beauty quark sample

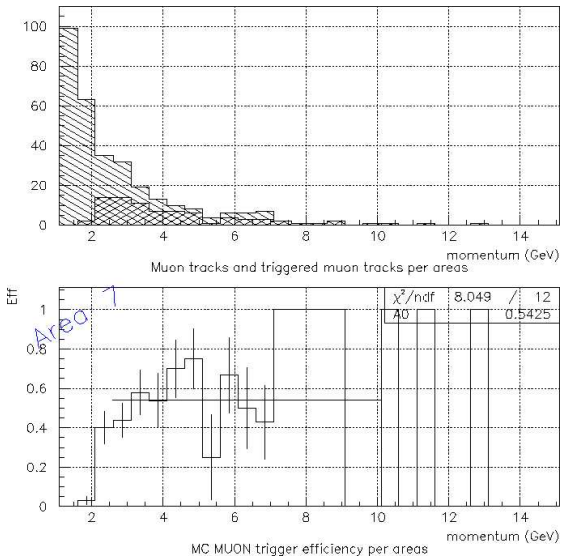

Figure 44: MC muon trigger efficiency results for BAC area 7 with the beauty quark sample

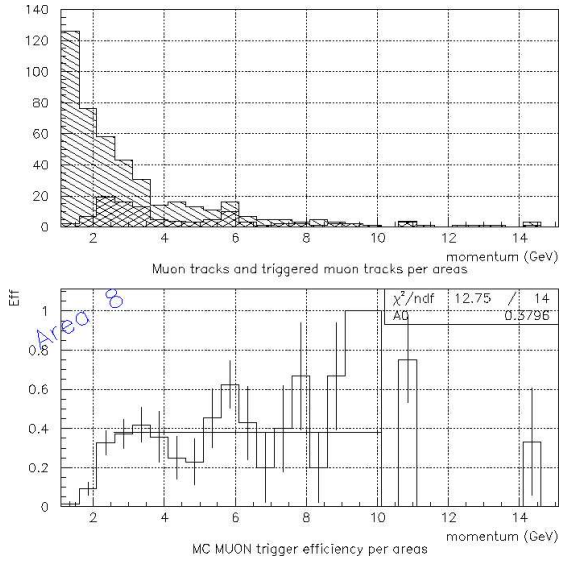

Figure 45: MC muon trigger efficiency results for BAC area 8 with the beauty quark sample

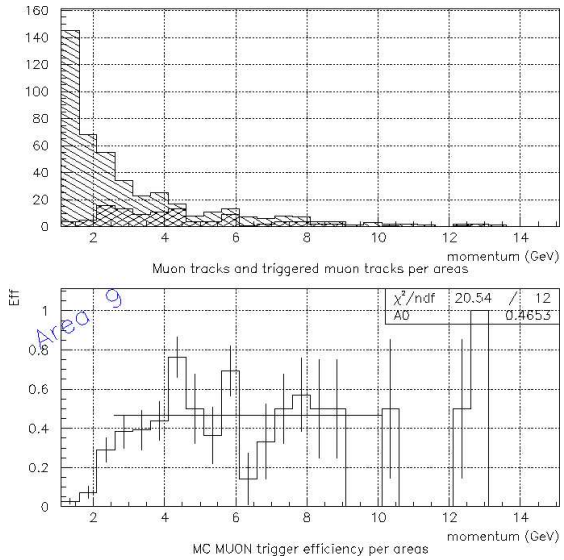

Figure 46: MC muon trigger efficiency results for BAC area 9 with the beauty quark sample

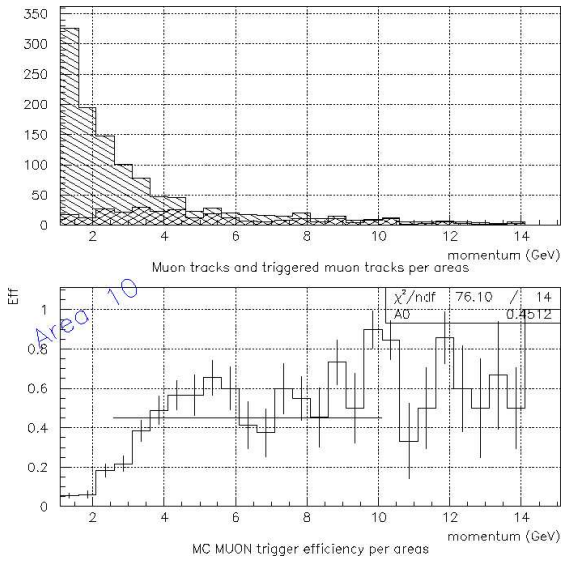

Figure 47: MC muon trigger efficiency results for BAC area 10 with the beauty quark sample

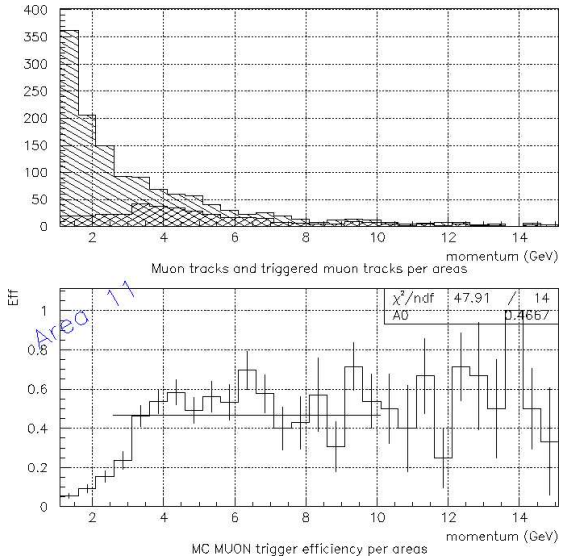

Figure 48: MC muon trigger efficiency results for BAC area 11 with the beauty quark sample

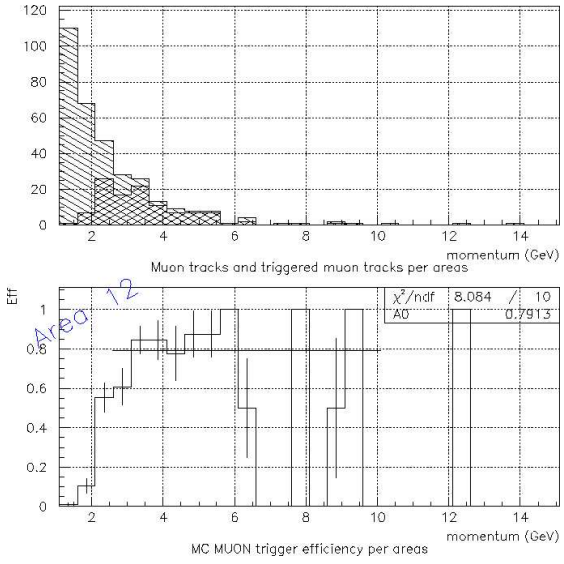

Figure 49: MC muon trigger efficiency results for BAC area 12 with the beauty quark sample

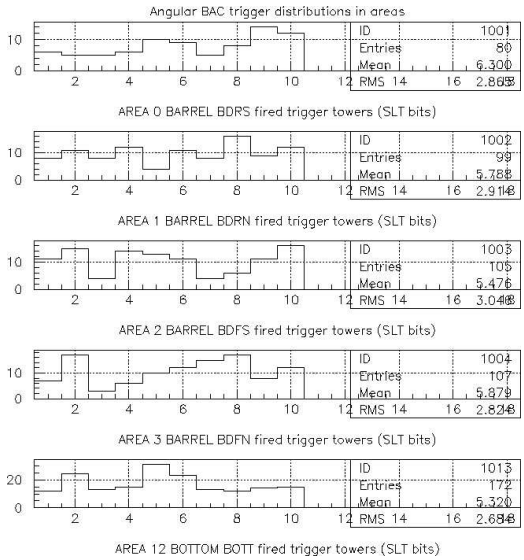

Figure 50: MC muon trigger angular distributions for Areas 0-4 and 12 with the beauty quark sample

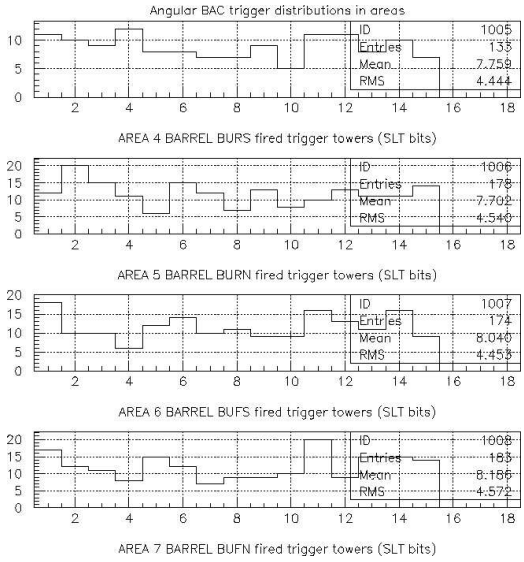

Figure 51: MC muon trigger angular distributions for Areas 4-7 with the beauty quark sample

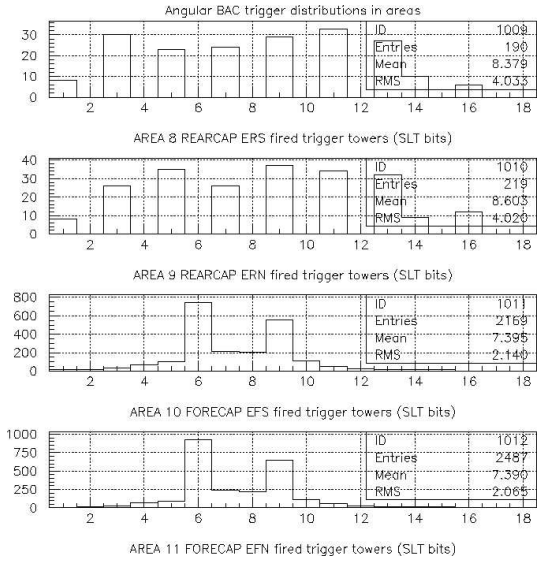

Figure 52: MC muon trigger angular distributions for Areas 8-11 with the beauty quark sample

7.3 Ψ' sample

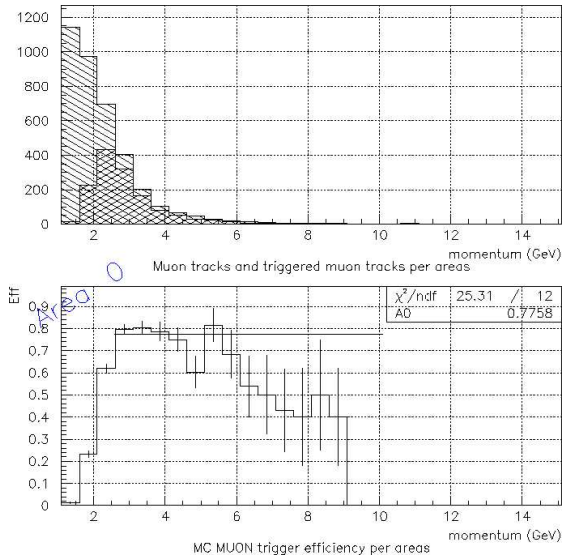

Figure 53: MC muon trigger efficiency results for BAC area 0 with Ψ' sample

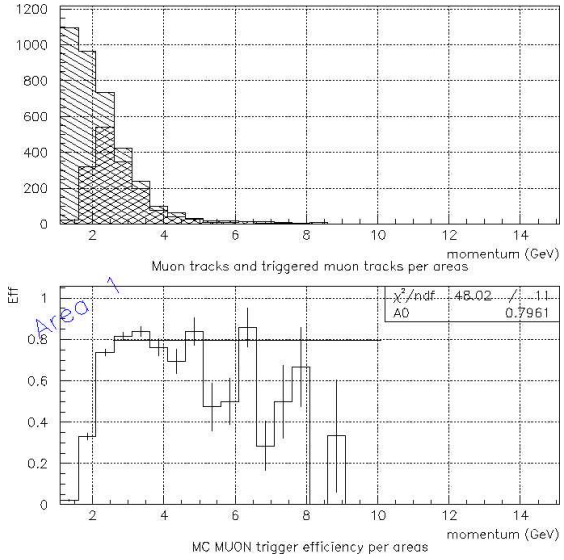

Figure 54: MC muon trigger efficiency results for BAC area 1 with Ψ' sample

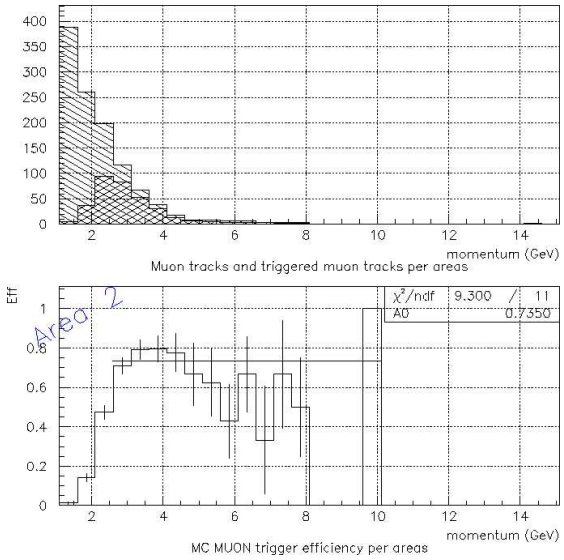

Figure 55: MC muon trigger efficiency results for BAC area 2 with Ψ' sample

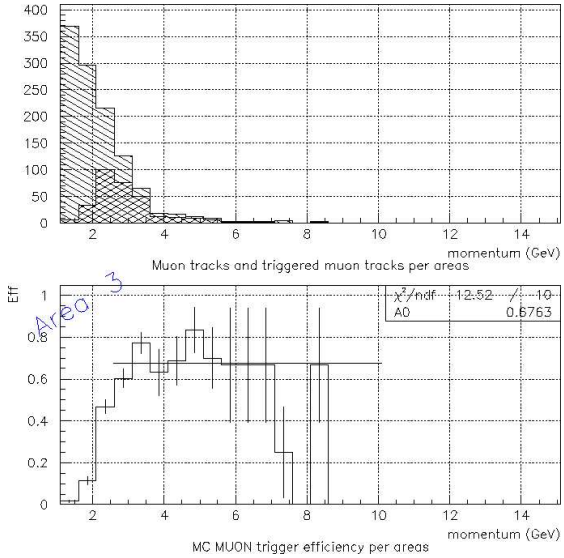

Figure 56: MC muon trigger efficiency results for BAC area 3 with Ψ' sample

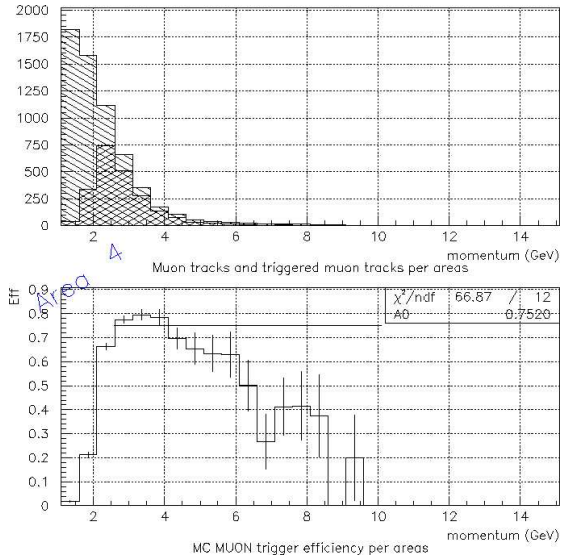

Figure 57: MC muon trigger efficiency results for BAC area 4 with Ψ' sample

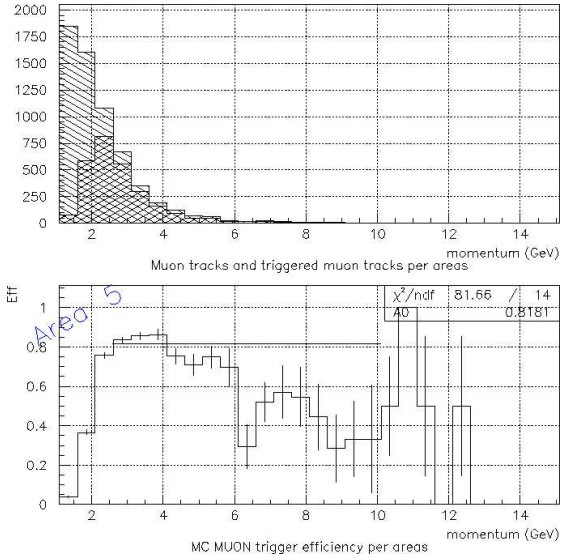

Figure 58: MC muon trigger efficiency results for BAC area 5 with Ψ' sample

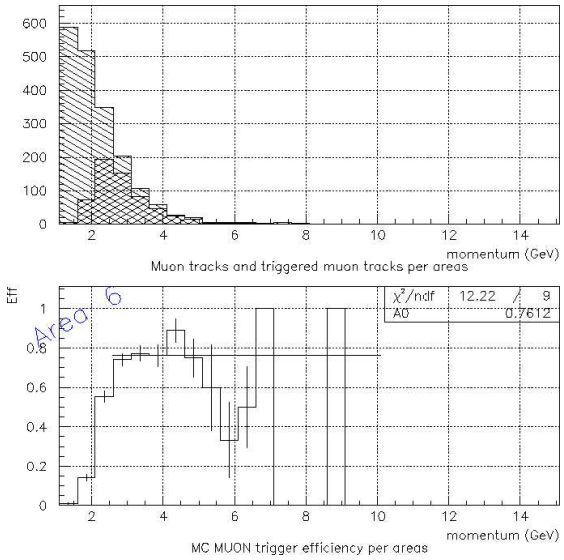

Figure 59: MC muon trigger efficiency results for BAC area 6 with Ψ' sample

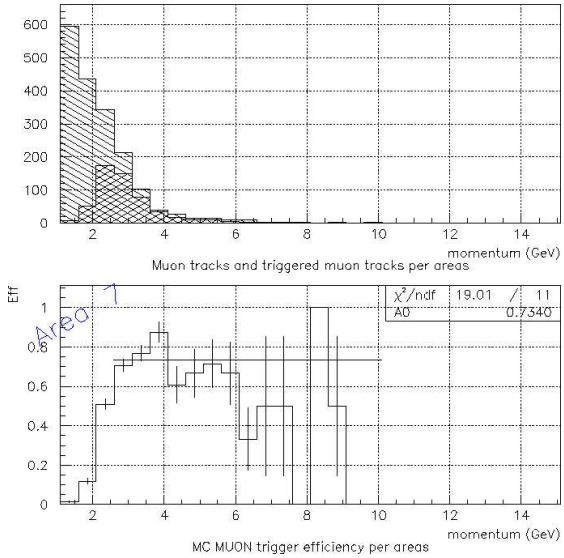

Figure 60: MC muon trigger efficiency results for BAC area 7 with Ψ' sample

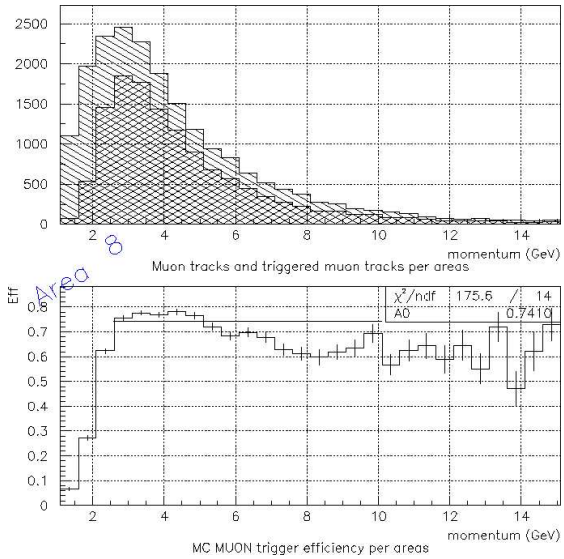

Figure 61: MC muon trigger efficiency results for BAC area 8 with Ψ' sample

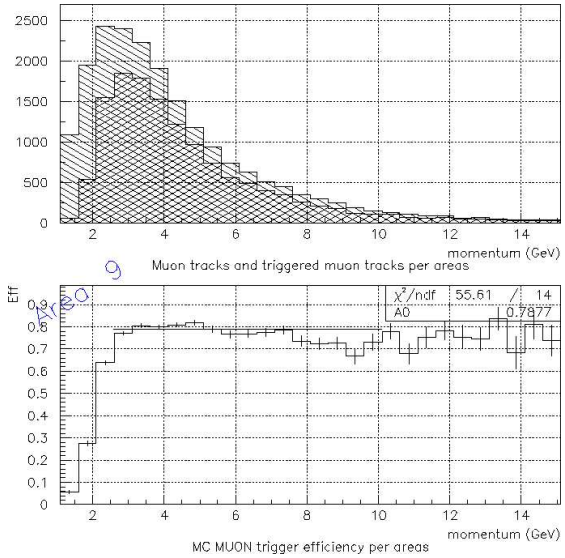

Figure 62: MC muon trigger efficiency results for BAC area 9 with Ψ′ sample

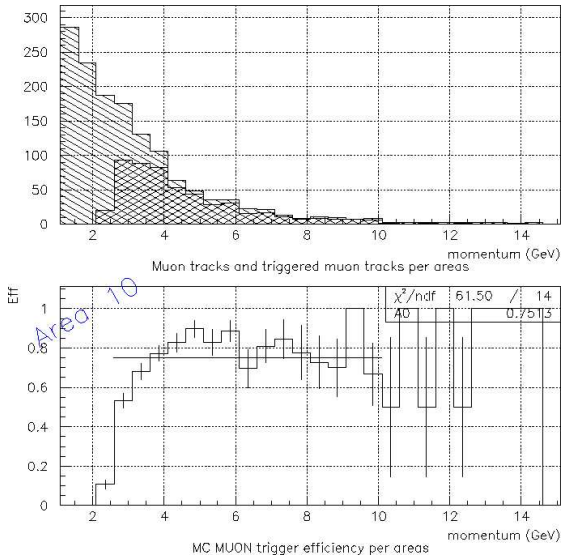

Figure 63: MC muon trigger efficiency results for BAC area 10 with Ψ′ sample

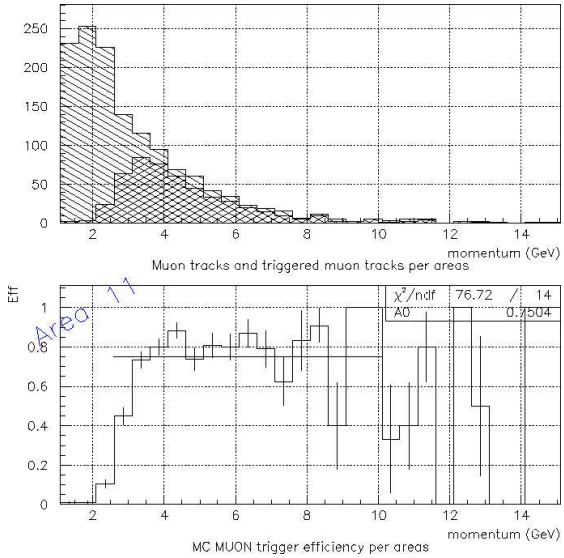

Figure 64: MC muon trigger efficiency results for BAC area 11 with Ψ' sample

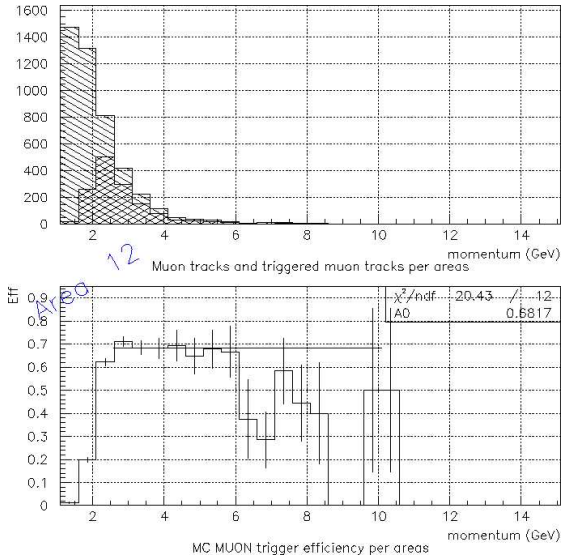

Figure 65: MC muon trigger efficiency results for BAC area 12 with Ψ' sample

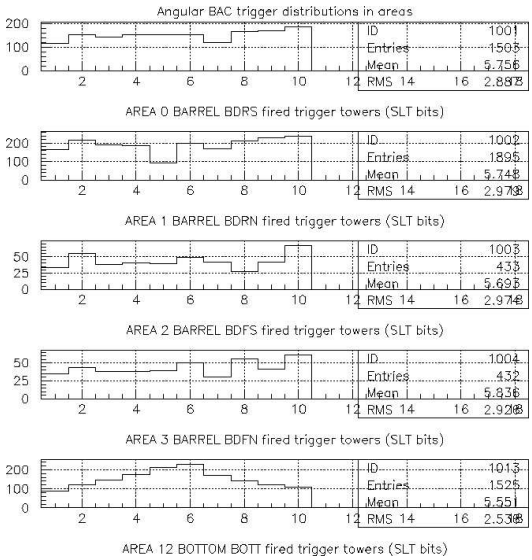

Figure 66: MC muon trigger angular distributions for Areas 0-4 and 12 with the Ψ′ sample

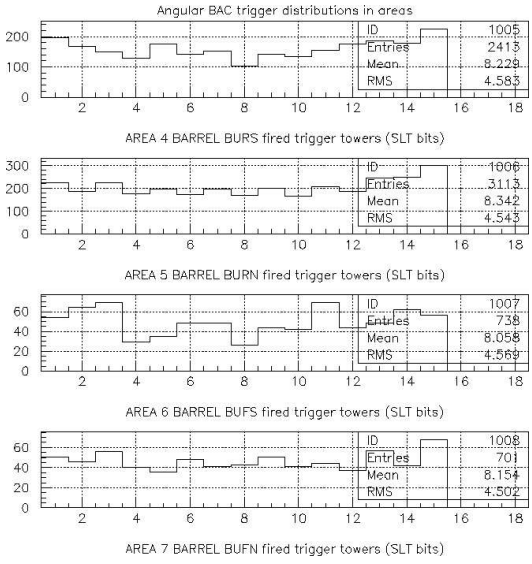

Figure 67: MC muon trigger angular distributions for Areas 4-7 with the Ψ′ sample

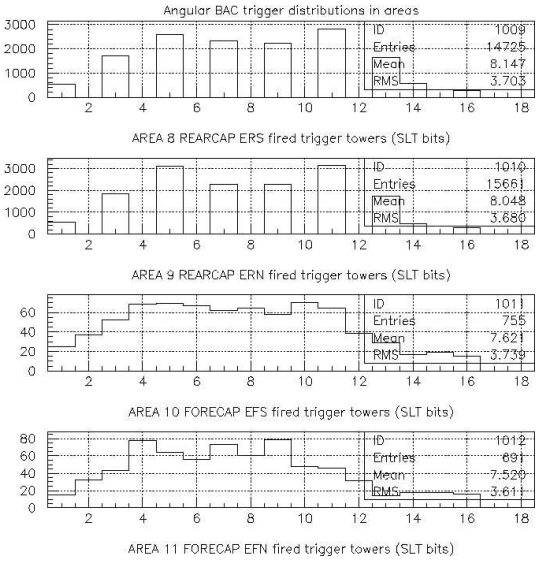

Figure 68: MC muon trigger angular distributions for Areas 8-11 with the Ψ' sample

7.4 J/Ψ sample

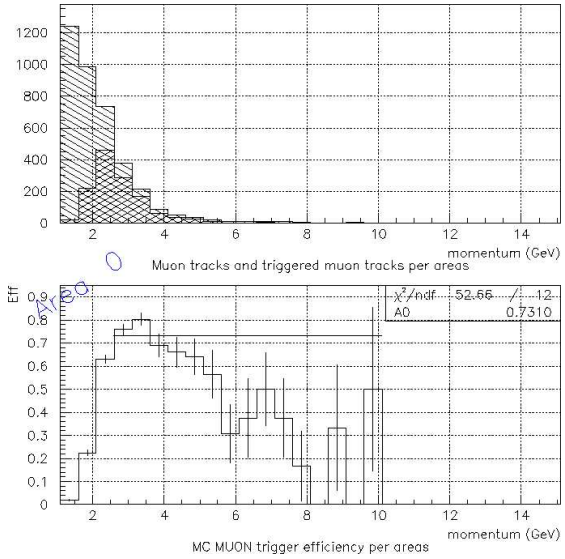

Figure 69: MC muon trigger efficiency results for BAC area 0 with the J/Ψ sample

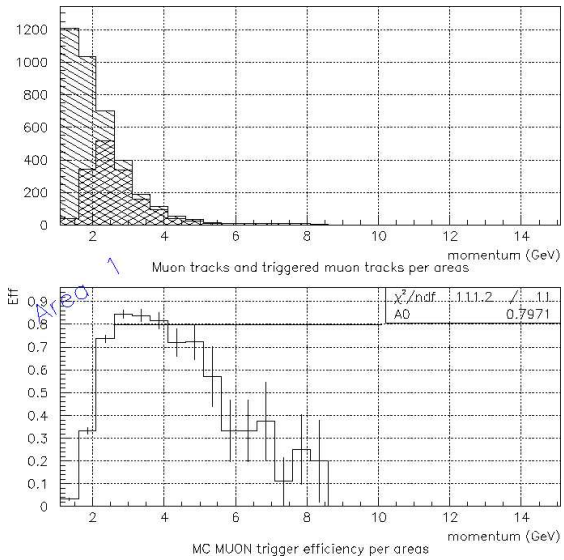

Figure 70: MC muon trigger efficiency results for BAC area 1 with the J/Ψ sample

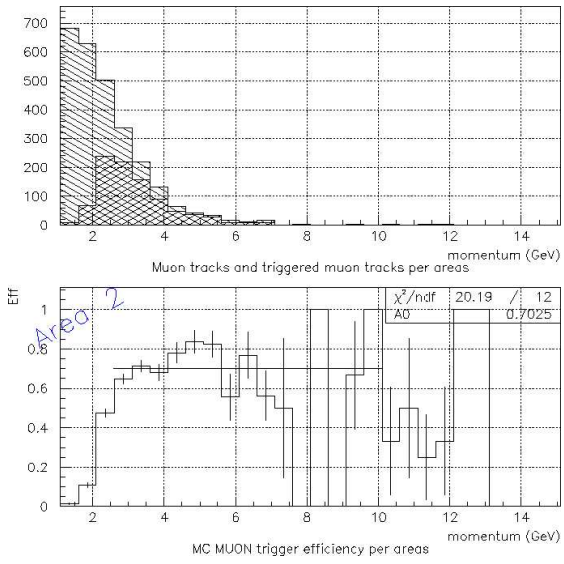

Figure 71: MC muon trigger efficiency results for BAC area 2 with the J/Ψ sample

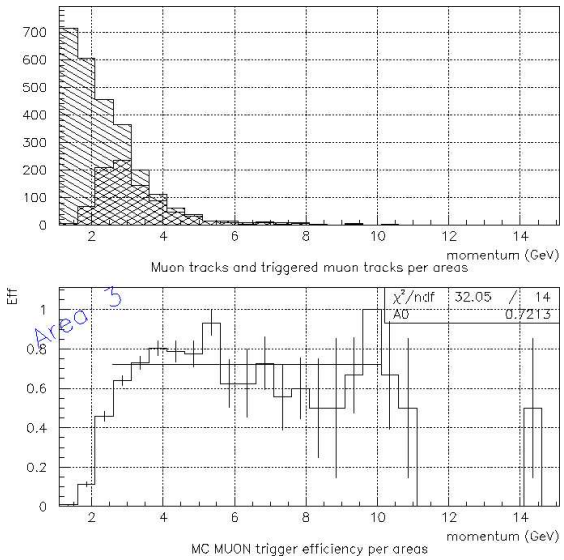

Figure 72: MC muon trigger efficiency results for BAC area 3 with the J/Ψ sample

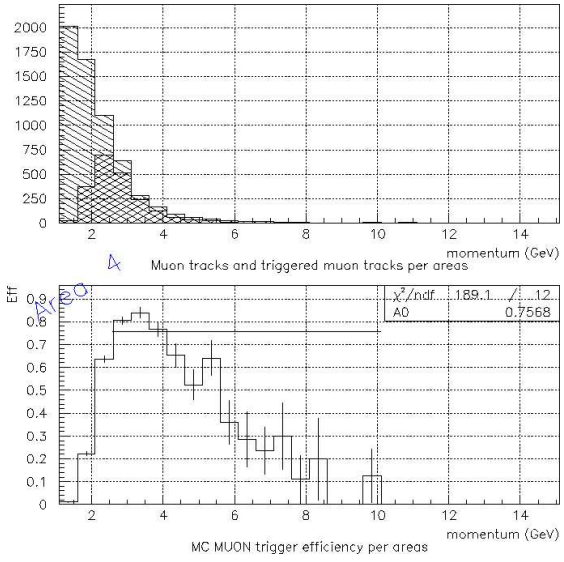

Figure 73: MC muon trigger efficiency results for BAC area 4 with the J/Ψ sample

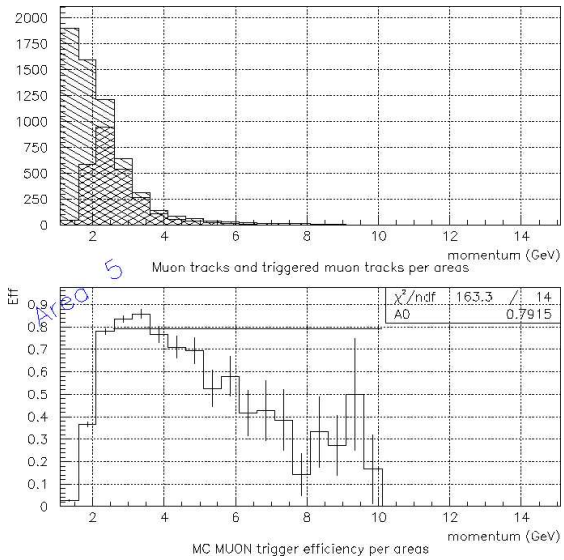

Figure 74: MC muon trigger efficiency results for BAC area 5 with the J/Ψ sample

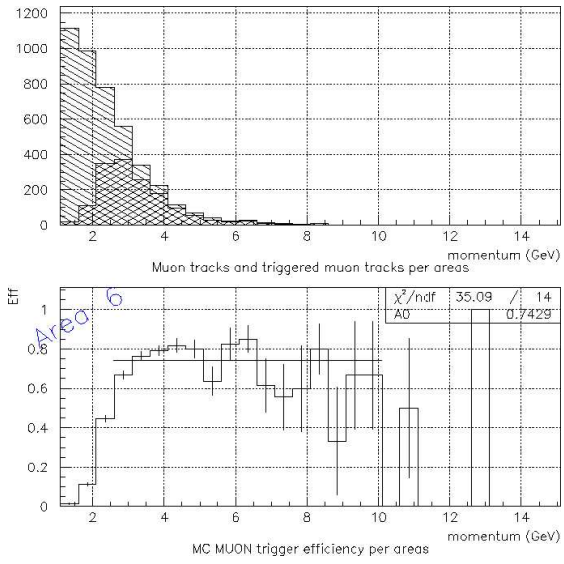

Figure 75: MC muon trigger efficiency results for BAC area 6 with the J/Ψ sample

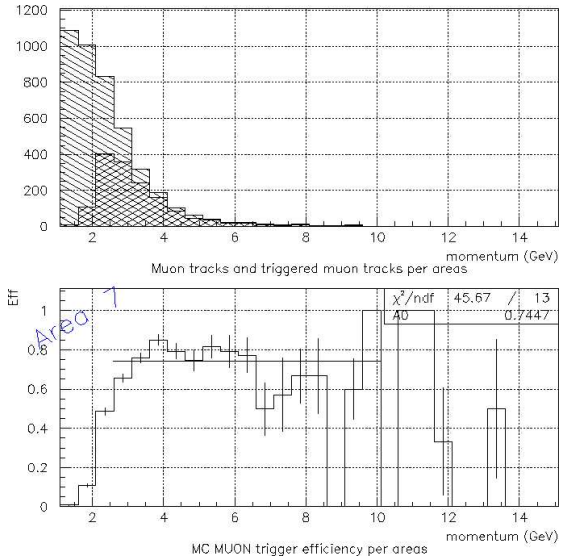

Figure 76: MC muon trigger efficiency results for BAC area 7 with the J/Ψ sample

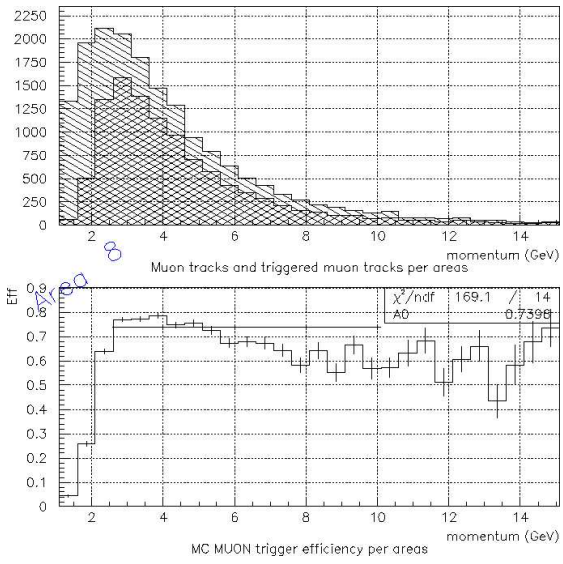

Figure 77: MC muon trigger efficiency results for BAC area 8 with the J/Ψ sample

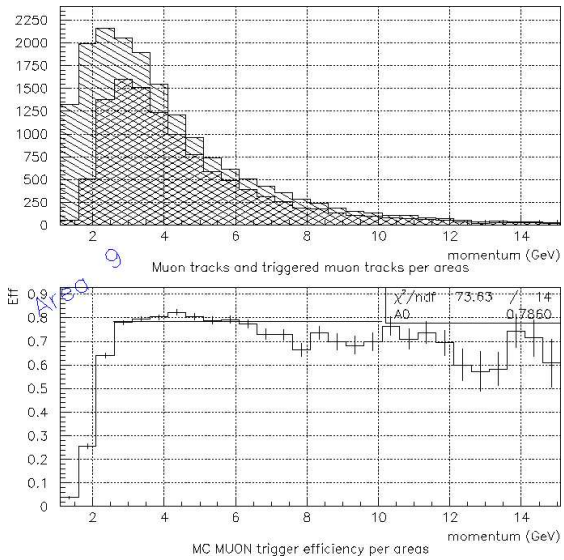

Figure 78: MC muon trigger efficiency results for BAC area 9 with the J/Ψ sample

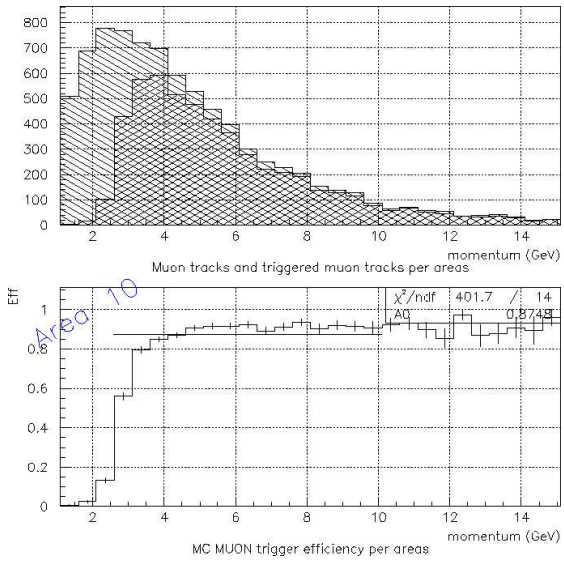

Figure 79: MC muon trigger efficiency results for BAC area 10 with the J/Ψ sample

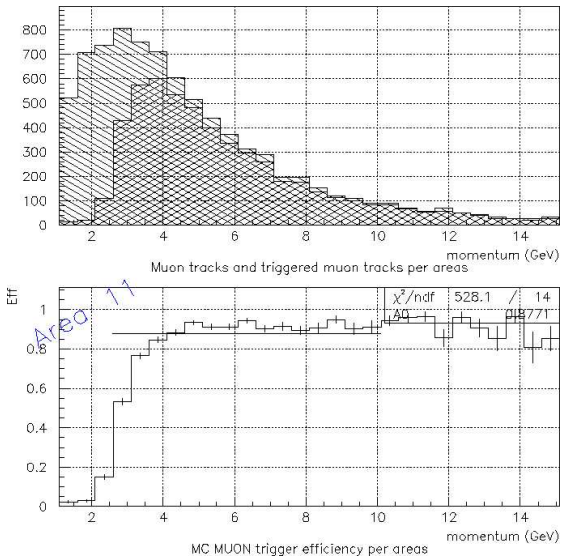

Figure 80: MC muon trigger efficiency results for BAC area 11 with the J/Ψ sample

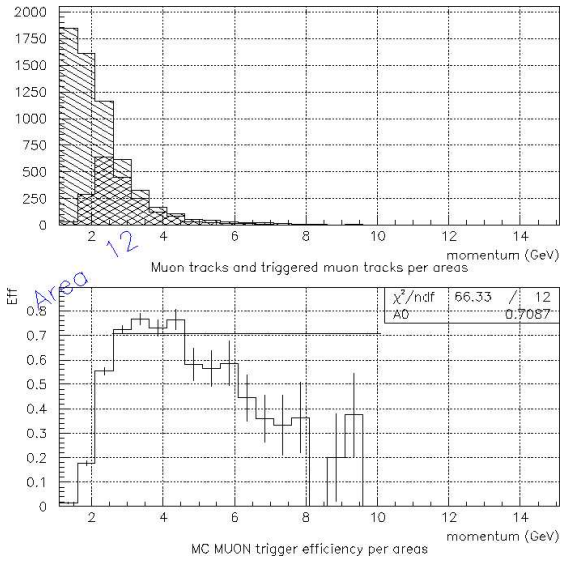

Figure 81: MC muon trigger efficiency results for BAC area 12 with the J/Ψ sample

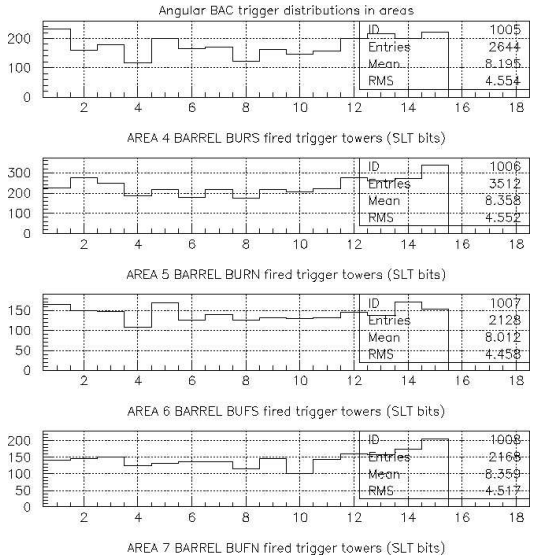

Figure 82: MC muon trigger angular distributions for Areas 0-4 and 12 with the J/Ψ sample

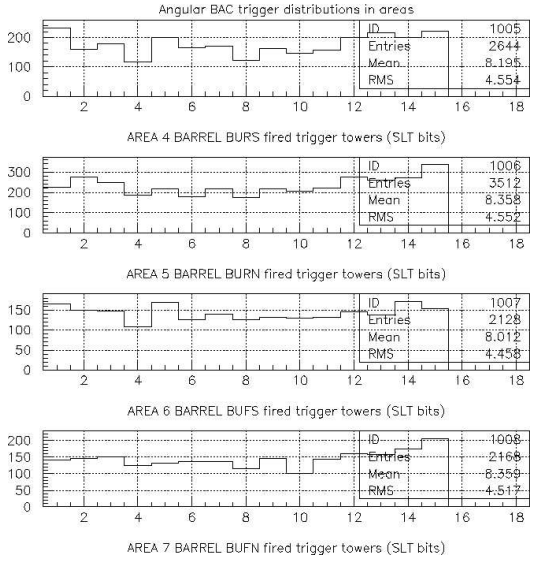

Figure 83: MC muon trigger angular distributions for Areas 4-7 with the J/Ψ sample

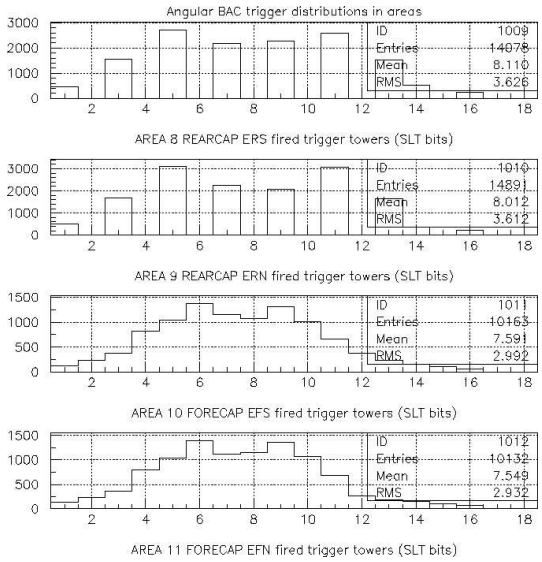

Figure 84: MC muon trigger angular distributions for Areas 8-11 with the J/Ψ sample

7.5 Elastic Bethe-Heitler process sample

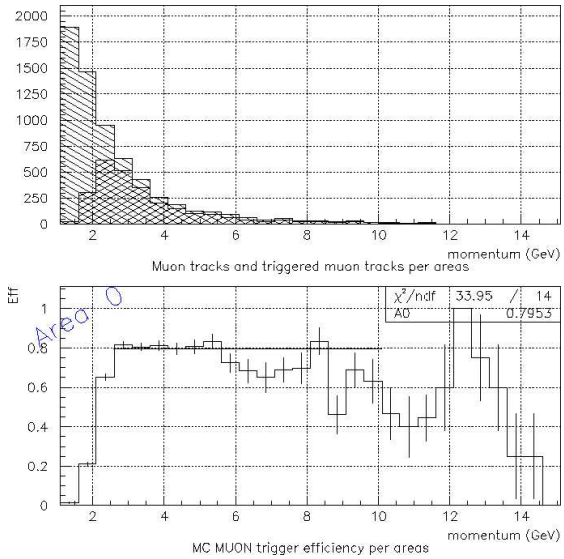

Figure 85: MC muon trigger efficiency results for BAC area 0 with the elastic Bethe-Heitler sample

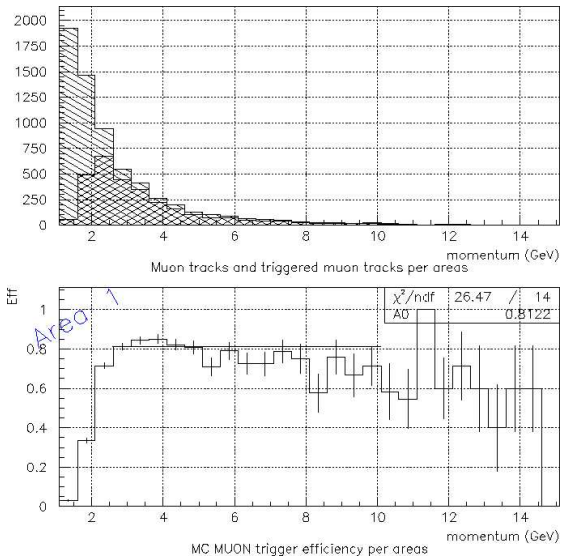

Figure 86: MC muon trigger efficiency results for BAC area 1 with the elastic Bethe-Heitler sample

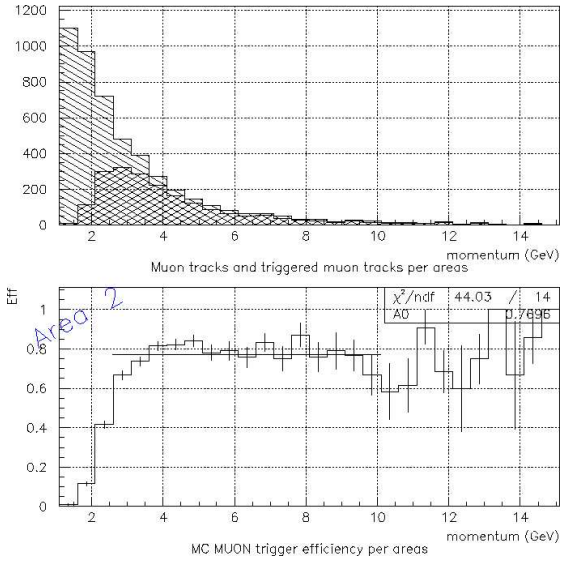

Figure 87: MC muon trigger efficiency results for BAC area 2 with the elastic Bethe-Heitler sample

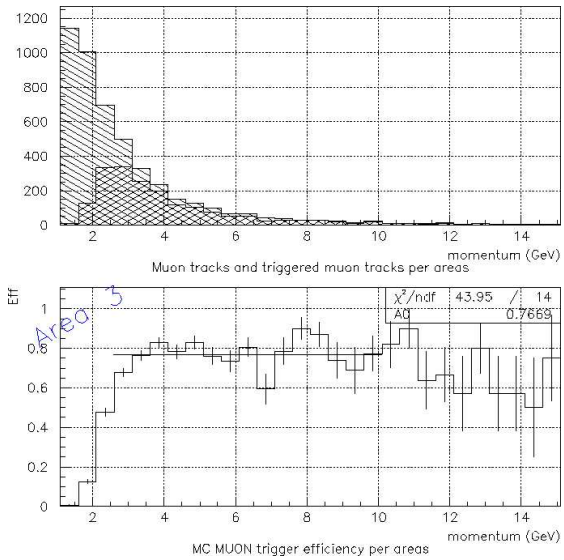

Figure 88: MC muon trigger efficiency results for BAC area 3 with the elastic Bethe-Heitler sample

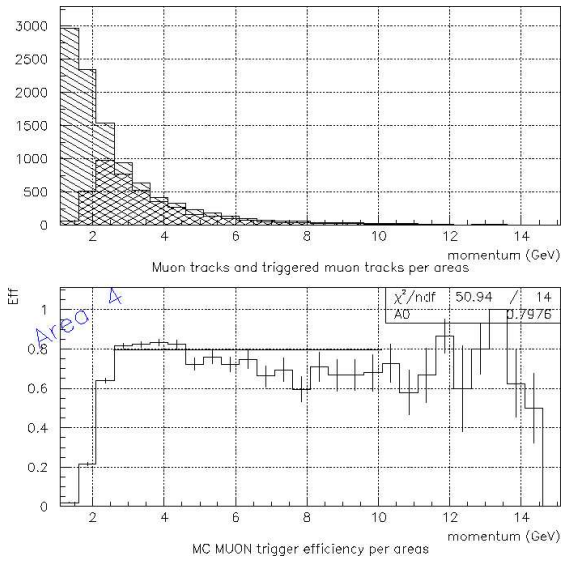

Figure 89: MC muon trigger efficiency results for BAC area 4 with the elastic Bethe-Heitler sample

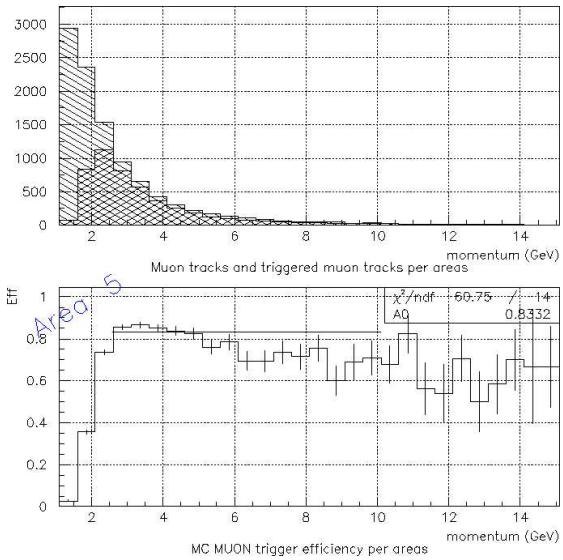

Figure 90: MC muon trigger efficiency results for BAC area 5 with the elastic Bethe-Heitler sample

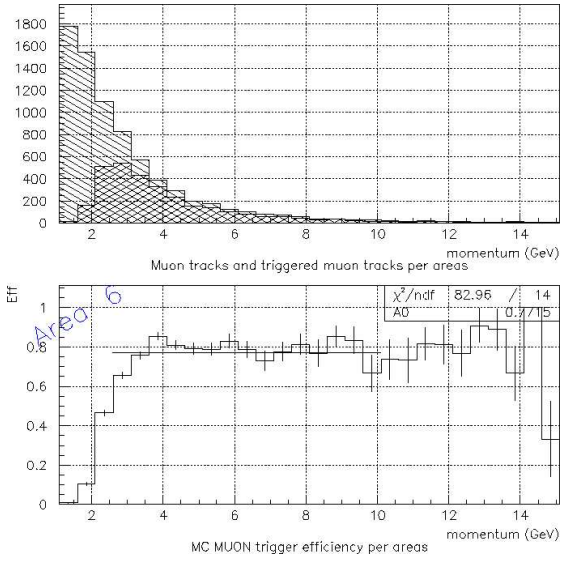

Figure 91: MC muon trigger efficiency results for BAC area 6 with the elastic Bethe-Heitler sample

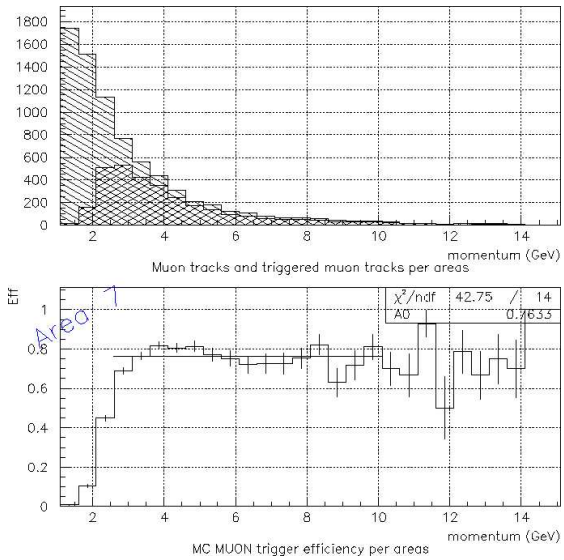

Figure 92: MC muon trigger efficiency results for BAC area 7 with the elastic Bethe-Heitler sample

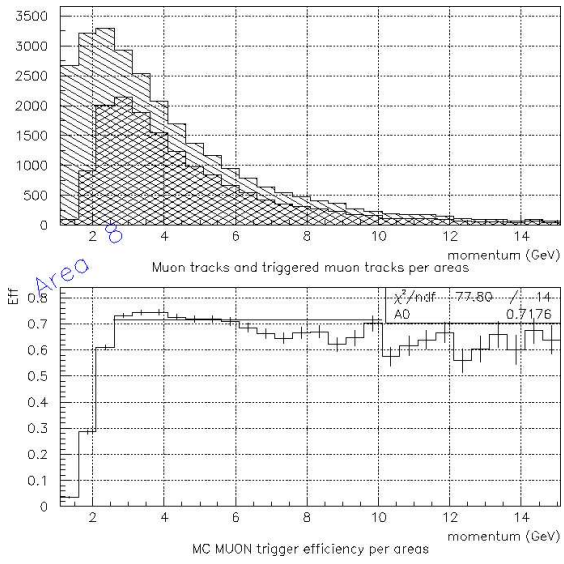

Figure 93: MC muon trigger efficiency results for BAC area 8 with the elastic Bethe-Heitler sample

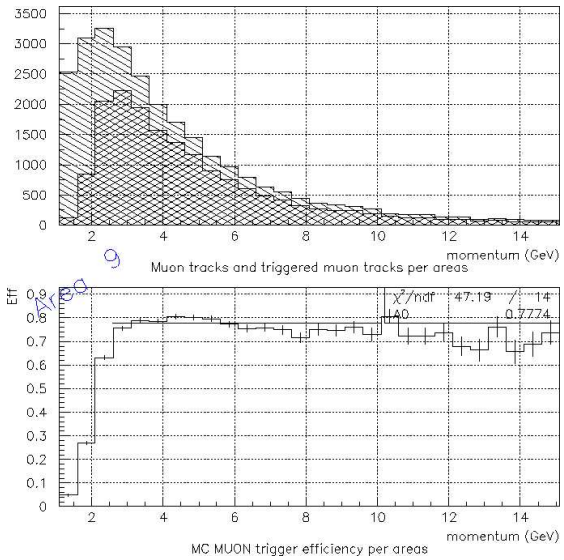

Figure 94: MC muon trigger efficiency results for BAC area 9 with the elastic Bethe-Heitler sample

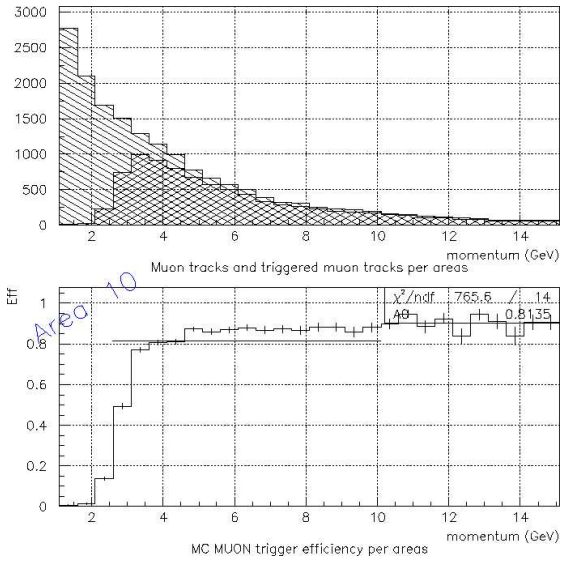

Figure 95: MC muon trigger efficiency results for BAC area 10 with the elastic Bethe-Heitler sample

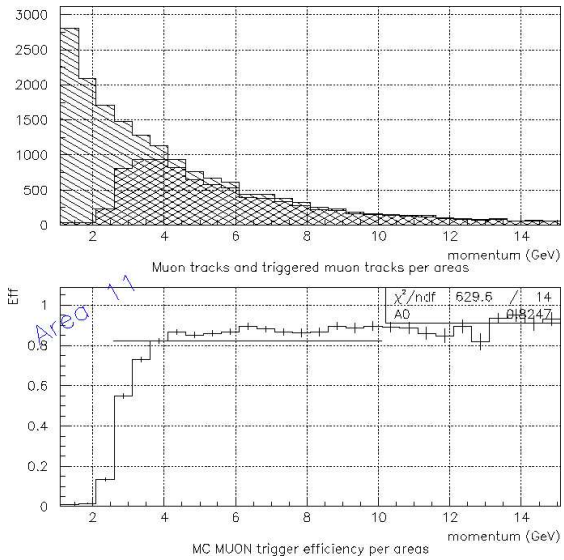

Figure 96: MC muon trigger efficiency results for BAC area 11 with the elastic Bethe-Heitler sample

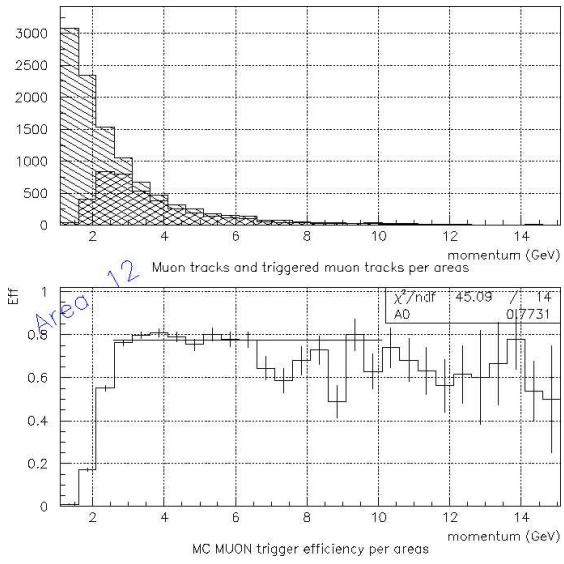

Figure 97: MC muon trigger efficiency results for BAC area 12 with the elastic Bethe-Heitler sample

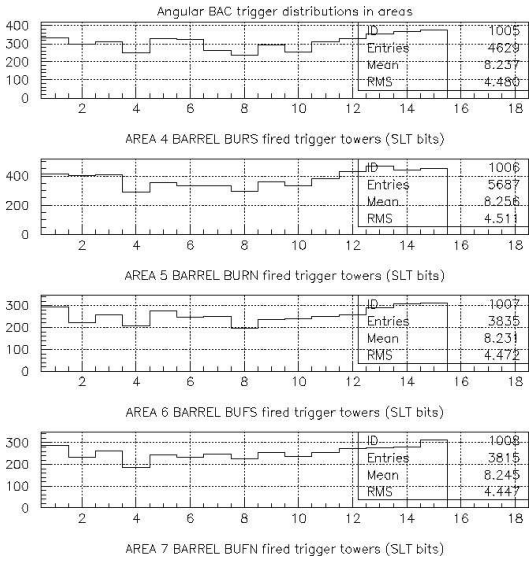

Figure 98: MC muon trigger angular distributions for Areas 4-7 with the elastic Bethe-Heitler sample

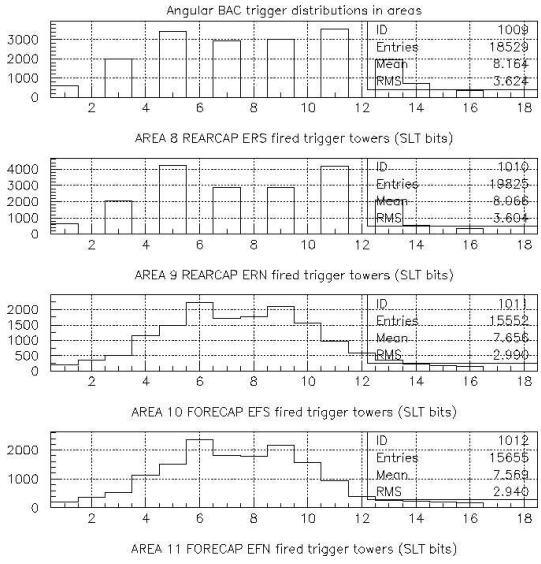

Figure 99: MC muon trigger angular distributions for Areas 8-11 with the elastic Bethe-Heitler process sample

Bibliography

[1] The ZEUS Collaboration, *HERA Collider Physics*, DESY 98-192

[2] The ZEUS Collaboration, *The ZEUS Detector*, Status Report, 1993

[3] H. Uijterwaal, *The Global Second Level Trigger for ZEUS*, PhD thesis, Amsterdam, 1992

[4] P.Pluciński, et al., *Trigger of the Backing Calorimeter for ZEUS Experiment*, Proceedings of SPIE, Bellingham, WA, USA, Vol. 5125, 2003

[5] G. Grzelak et al., *Overview of the Backing Calorimeter after the ZEUS Detector Upgrade*, Proceedings of SPIE, Bellingham, WA, USA, Vol. 5125, 2003

[6] G. Bałuka, G. Grzelak, R. Kupczak, T. Jeżyński, *System Akwizycji Danych BAC*, DESY Hamburg, 2001

[7] J. Sztuk, *Rekonstrukcja przypadków produkcji J/Ψ i Ψ' w głęboko-nieelastycznym rozpraszaniu $e^{\pm}p$*, praca magisterska, Warszawa, 2000

[8] P. Łużniak, *Pomiar pędu mionów zatrzymujących sie w kalorymetrze BAC (w eksperymancie ZEUS przy akceleratorze HERA)*, praca magisterska, Łódź, 2002

[9] J. Tomaszewska, *Produkcja wysokoenergetycznych par mionów w eksperymencie ZEUS*, praca magisterska, Warszawa, 2000

[10] B.R. Martin, G.Shaw, *Particle Physics*, Wiley and Sons, 1992

[11] V. Chiochia, *Measurment of beauty quark production in deep inelastic scattering at HERA*, PhD thesis, Hamburg, 2003

[12] M. Turcato, *Measurment of beauty photoproduction at HERA*, PhD thesis, Padova, 2002

[13] A. Kappes, *Measurment of $e^-p \to e^-X$ differential cross sections at high Q^2 and of the structure function xF_3 with ZEUS at HERA*, PhD thesis, Bonn, 2001

[14] A.D. Tapper, *Measurment of charged current deep inelastic scattering cross sections using the ZEUS detector at HERA*, PhD thesis, London, 2001

[15] R.K. Ellis et al., Nucl. Phys. **B 152** 285, 1989

[16] B. Smalska, *Measurment of the proton diffractive structure functions in the ZEUS experiment*, PhD thesis, Warsaw, 2001
[17] A. Longhin, *Measurment of beauty production at HERA with a $D^\star + \mu$ tag*, PhD thesis, Padova, 2003
[18] K. Hagiwara et al., Phys. Rev. D **66**, (2002)
[19] T. Regge, Nuovo Cimento **14**, 951 (1959)
[20] T. Regge, Nuovo Cimento **18**, 947 (1960)
[21] J. Gajewski, M. Gromisz, G.Grzelak, *BACFLT, FLSBAC ZGANA energy trigger codes*
[22] M. Własenko, *BACFLT ZGANA muon trigger codes*
[23] J. Ciborowski, G. Grzelak, K. Klimek, P. Łużniak, P. Pluciński, M. Turcato, *direct information*
[24] J. Malka, *Analiza Układu wyzwalania kalorymetru uzupełniającego BAC w ekperymencie ZEUS*, praca magisterska, Łódź, 2004
[25] The ZEUS Collaboration, *A ZEUS next-to-leading-order QCD analysis of data on deep inelastic scattering*, Physical Review D 67, 012007 (2002)
[26] http://www-zeus.desy.de/physicsgroups.php3
[27] http://www-h1.desy.de/
[28] M. Klein, *Physics with H1 at HERA II*, H1 Collaboration Meeting, CPPM Marseille, September 16th, 2003
[29] ZEUS Collaboration, *Measurment of the photon-proton total cross section at a center-of-mass energy of 209 GeV at HERA*, Nucl. Phys., B627 (2002) 3-28
[30] D.H. Perkins, *Introduction to High Energy Physics*, Addison-Wesley, 1987
[31] B. List, A. Mastroberardino, *DIFFVM - A Monte Carlo Generator for Diffractive Processes in ep Scattering*, Hamburg (DESY) DESY-PROC-1992-02, p.396-404
[32] H. Jung, *The RAPGAP Monte Carlo for Deep Inelstaic Scattering, version 2.08*, Lund University, 1999, http://www.desy.de/ jung/rapgap.html
[33] H. Spiesberger, et al., *HERACLES: An Event Generator for ep Interactions at HERA Energies including Radiative Processes: version 1.0*, Comp. Phys. Comm 69 (1992) 155-172
[34] T. Abe, *GRAPE - Dilepton. A Generator for Dilepton Production in ep Collisions.* Comp. Phys. Comm 136 (2001) 126-147